Article

Immunity

Environmental enteric dysfunction induces regulatory T cells that inhibit local CD4+ T cell responses and impair oral vaccine efficacy

Graphical abstract

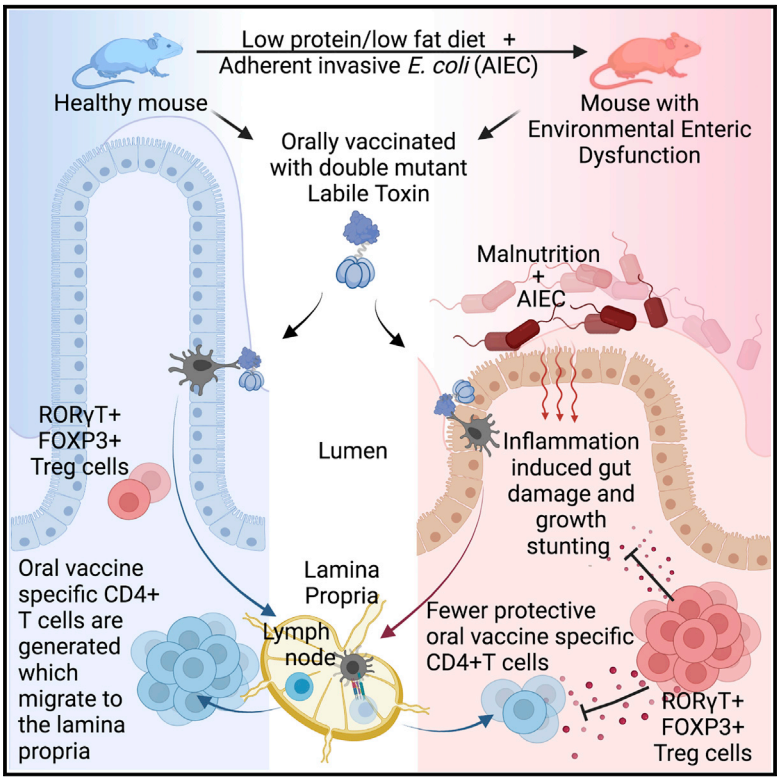

Highlights

- Mouse model mimics human EED, including stunting and intestinal inflammation
- EED causes an intestine-specific failure in oral vaccine-specific T cell responses
- EED induces intestinal microbiota-dependent RORγT^{+}FOXP3^{+} Treg T cells
- Depletion of Treg cells restores oral vaccine responses but increases stunting

Authors

Amrita Bhattacharjee, Ansen H.P. Burr, Abigail E. Overacre-Delgoffe, ..., Elizabeth B. Norton, Yasmine Belkaid, Timothy W. Hand

Correspondence

timothy.hand@chp.edu

In brief

Environmental enteric dysfunction (EED) is caused by chronic malnutrition and infection and is associated with stunting and reduced oral vaccine efficacy in children. Bhattacharjee et al. develop a mouse model of EED and reveal both oral vaccine failure and stunting is controlled by a localized increase in intestinal RORγT^{+}FOXP3^{+} regulatory T cells.

Bhattacharjee et al., 2021, Immunity *54*, 1745–1757
August 10, 2021
https://doi.org/10.1016/j.immuni.2021.07.005

CellPress

Immunity

CellPress

Article

Environmental enteric dysfunction induces regulatory T cells that inhibit local CD4+ T cell responses and impair oral vaccine efficacy

Amrita Bhattacharjee,[1] Ansen H.P. Burr,[1,2] Abigail E. Overacre-Delgoffe,[1] Justin T. Tometich,[1] Deyi Yang,[1,3] Brydie R. Huckestein,[2] Jonathan L. Linehan,[4,6] Sean P. Spencer,[4,7] Jason A. Hall,[4,8] Oliver J. Harrison,[4,9] Denise Morais da Fonseca,[4,10] Elizabeth B. Norton,[5] Yasmine Belkaid,[4] and Timothy W. Hand[1,2,11,*]

[1]R.K. Mellon Institute for Pediatric Research, Pediatrics Department, Infectious Disease Section, UPMC Children's Hospital of Pittsburgh, University of Pittsburgh, Pittsburgh, PA 15224 USA

[2]Program in Microbiology and Immunology, Department of Immunology, University of Pittsburgh, School of Medicine, Pittsburgh, PA 15261, USA

[3]Central South University, Xiangya School of Medicine, Changsha, PRC

[4]Metaorganism Immunity Section, Laboratory of Immune System Biology, National Institute of Allergy and Infectious Disease, National Institutes of Health, Bethesda, MD, USA

[5]Department of Microbiology and Immunology, Tulane University School of Medicine, New Orleans, LA, USA

[6]Present address: Genentech Inc., South San Francisco, CA, USA

[7]Present address: Department of Microbiology and Immunology, Stanford University School of Medicine, Palo Alto, CA, USA

[8]Present address: ArsenalBio Inc., San Francisco, CA, USA

[9]Present address: Benaroya Research Institute, Seattle, WA, USA

[10]Present address: Department of Immunology, Institute of Biomedical Sciences, University of São Paulo, São Paulo, Brazil

[11]Lead contact

*Correspondence: timothy.hand@chp.edu

https://doi.org/10.1016/j.immuni.2021.07.005

SUMMARY

Environmental enteric dysfunction (EED) is a gastrointestinal inflammatory disease caused by malnutrition and chronic infection. EED is associated with stunting in children and reduced efficacy of oral vaccines. To study the mechanisms of oral vaccine failure during EED, we developed a microbiota- and diet-dependent mouse EED model. Analysis of *E. coli*-labile toxin vaccine-specific $CD4^+$ T cells in these mice revealed impaired $CD4^+$ T cell responses in the small intestine and but not the lymph nodes. EED mice exhibited increased frequencies of small intestine-resident $ROR\gamma T^+FOXP3^+$ regulatory T (Treg) cells. Targeted deletion of $ROR\gamma T$ from Treg cells restored small intestinal vaccine-specific CD4 T cell responses and vaccine-mediated protection upon challenge. However, ablation of $ROR\gamma T^+FOXP3^+$ Treg cells made mice more susceptible to EED-induced stunting. Our findings provide insight into the poor efficacy of oral vaccines in EED and highlight how $ROR\gamma T^+FOXP3^+$ Treg cells can regulate intestinal immunity while leaving systemic responses intact.

INTRODUCTION

Oral vaccines are an effective mechanism to provide immunity against infection in the gastrointestinal tract and are used to prevent the spread of enteric viral and bacterial infections (Vela Ramirez et al., 2017). Bacterial enterotoxins, such as the *E. coli* heat labile toxin (LT), have the potential to be excellent oral vaccines because they possess intrinsic adjuvant activity. Attenuated enterotoxins are currently in trials as both adjuvants and vaccines against various enteric infections (Clements and Norton, 2018; Harro et al., 2019; Norton et al., 2011; Shaikh et al., 2020). Oral vaccines can induce long-lived intestinal-resident $CD4^+$ T cells and IgA^+ plasma B cells, which mediate protection at the site of infection (Bemark et al., 2016; Clements and Norton, 2018; Pasetti et al., 2011). How intestinal-resident T and B cells develop and are regulated after oral vaccination and the role of the local intestinal microbiota in their biology is not completely understood.

Intestinal immunity requires a balance between restricting infectious microorganisms and avoiding persistent activation by the gut microbiota to prevent autoinflammatory disorders such as inflammatory bowel disease. This equilibrium is complicated by the ever-changing environment of the intestine, where the host-microbiota relationship can be modified by shifts in diet and infection (Carmody et al., 2015; Cotillard et al., 2013; Hand, 2016). Diet-driven microbial shifts are associated with a variety of chronic diseases, and therapies that restore health to the microbiota can influence effective treatments (Blanton et al., 2016; Hand et al., 2016; Ridaura et al., 2013; Turnbaugh et al., 2006). Regardless of the trigger, microbial dysbiosis

affects the immune response both locally, at barrier sites, and systemically, contributing to inflammatory disease (Henao-Mejia et al., 2012; Honda and Littman, 2016).

Intestinal regulatory T (Treg) cells play an important role in shaping immune responses to mucosally encountered antigens, such as those derived from oral vaccines. The role of Treg cells in oral vaccination is complex, because in contrast to their regulation of T cell responses Treg cells support the generation of IgA-producing B cells, particularly within Peyer's patches (PPs) (Cong et al., 2009; Gribonika et al., 2019; Kawamoto et al., 2014; Tsuji et al., 2009). Intestinal Treg cells can be categorized by markers that differ according to the source of the antigens that they are specific to, where Treg cells responding to self-antigens are Neuropilin 1^+, RAR-related orphan receptor γ t^-(NRP1^+RORγT^-), those responding to microbiome-derived antigens are NRP1^- RORγT^+, and those responding to food are negative for both molecules (Kim et al., 2016; Ohnmacht et al., 2015; Sefik et al., 2015; Weiss et al., 2012; Xu et al., 2018). The balance of Treg and T helper cells in the intestine is important because inflammatory diseases have been associated with increased frequencies of Th1 and Th17 cells and decreased Treg cells (Leung et al., 2014; Lochner et al., 2008). Whether Treg or T helper cell differentiation dominates the immune response to intestinal bacteria is dependent both upon the biology of the bacteria and extrinsic environmental factors and is likely important to the efficacy of oral vaccination (Ansaldo et al., 2019; Chai et al., 2017; Chiaranunt et al., 2018; Hand et al., 2012; Xu et al., 2018; Zhao et al., 2017).

Environmental enteric dysfunction (EED) is a gastrointestinal inflammatory disease most commonly seen in children in resource-poor settings that contributes to developmental stunting (Keusch et al., 2014; Korpe and Petri, 2012). While EED is rare in resource-rich countries, approximately 150 million children are at risk worldwide. EED is caused by a combination of malnutrition and chronic intestinal infection and is characterized by microbial dysbiosis, lymphocytic infiltration, and a flattening of villi in the small intestine, which causes malabsorption due to reduced surface area (Korpe and Petri, 2012). Areas where EED is endemic are also associated with a reduced efficacy of oral vaccines (Naylor et al., 2015). There are several factors that may contribute to oral vaccine failure in resource-poor countries including EED-induced disruption of intestinal immunity (Bhattacharjee and Hand, 2018; Di Luccia et al., 2020; Naylor et al., 2015).

To identify how EED disrupts intestinal immune responses and reduces the efficacy of oral vaccines, we developed a mouse model of EED dependent upon malnutrition and intestinal colonization with adherent invasive *E.coli*. This model recapitulated multiple aspects of human EED, including growth stunting, intestinal villi shortening, and reduced intestinal barrier function. Upon oral vaccination, EED-affected mice exhibited a near-complete block in the accumulation of intestinal oral vaccine-specific $CD4^+$ T cells while responses in secondary lymphoid tissue were intact. This failure of vaccine-specific $CD4^+$T cell responses in the intestine was accompanied by a coincident increase in the number and function of RORγT^+ Treg cells in the intestine, and ablation of these cells restored oral vaccine efficacy. However, depletion of RORγT^+ Treg cells increased the severity of EED-induced stunting, indicating the importance of these cells in regulating chronic intestinal inflammation. Taken together, our data support the idea that oral vaccine failure in EED is a consequence of a localized intestinal immune regulation and uncovers a modular structure for tissue and systemic immune responses.

RESULTS

Murine EED is associated with weight loss, growth stunting, and increased intestinal permeability

We developed an animal model of EED to replicate the intestinal inflammation, barrier defects, and growth stunting associated with the disease in children. Existing mouse models require changes to both the diet and microbiota to induce EED-like symptoms, and affected animals show an enrichment for *Enterobacteriaceae* in the mucus layer of the small intestine (Brown et al., 2015; Kau et al., 2015). We hypothesized that a combination of low protein/fat diet and colonization with an adherent-invasive *E. coli* (AIEC) isolate that intrinsically associated with the small intestinal epithelium would be sufficient to induce EED (Rolhion and Darfeuille-Michaud, 2007). The *E. coli* isolate "CUMT8" was chosen because it is derived from mice, adheres to the small intestinal epithelium, and "blooms" under inflammatory conditions (Craven et al., 2012; Dogan et al., 2014). To control for diet and microbiota, our experiments had four groups: (1) isocaloric (ISO) controls fed a diet with sufficient fat and protein, (2) malnourishment (MAL) controls fed a low protein/fat chow, (3) CUMT8 *E. coli* colonized controls (MT8) on normal protein/fat diet, and (4) mice that receive both low protein/fat chow and CUMT8 *E. coli*, which could develop EED-like disease (EED) (Figure 1A). Mice were initiated onto their respective diets at 3 weeks of age and colonized with CUMT8 *E. coli* 16, 18, and 20 days later. All mice were fed an equal amount of food (by calories) to prevent the mice that were fed the low fat/protein diet from over-eating. As expected, mice fed with the MAL diet (MAL and EED) gained weight more slowly than mice fed the isocaloric control diet (Figure 1B). Independent of diet, administration of CUMT8 *E. coli* temporarily slowed the growth of mice (MT8 and EED), and the combination of low protein/fat diet and CUMT8 *E. coli* led to a reduction in growth of EED mice compared to controls (Figure 1B; Figure S1A). EED mice also exhibited other signs of growth stunting, as evidenced by reduced tail lengths (Figure 1C). In humans, EED is characterized by a reduction in the length of the intestinal villi ("blunting"), increased immune cell infiltration, elevated intestinal inflammation, and reduced intestinal barrier function (Korpe and Petri, 2012). Histological analysis of the terminal ileum revealed that EED mice, but not any of the controls, exhibited villous blunting and lymphocytic infiltration (Figures 1D and 1E). The small intestine of mice on the EED protocol was more inflamed, as indicated by increased expression inflammatory cytokines (interferon gamma and tumor necrosis factor alpha and the anti-bacterial gene Lcn2 (Figures S1B and S1C) (Chen et al., 2020; Haberman et al., 2021; Watanabe and Petri, 2016). EED mice also exhibited decreased intestinal barrier function as measured by the detection of orally administered FITC-dextran particles in the blood (Figure 1F) (Keusch et al., 2014). To test whether colonization with an adherent/invasive strain of *E. coli* was required for the development of EED-like disease, we substituted CUMT8 *E. coli* for either a sessile commensal *E. coli* "ECMB" or a human

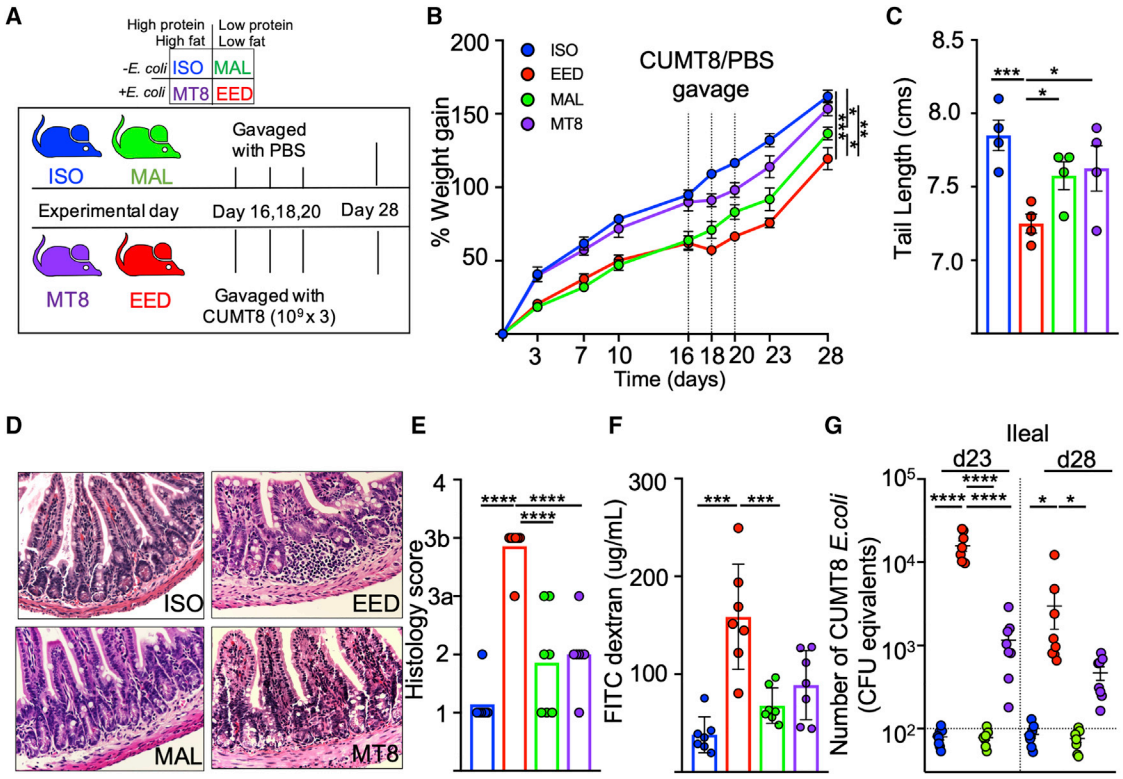

Figure 1. Murine EED is associated with weight loss, growth stunting, and increased intestinal permeability

(A) Schematic of the EED protocol. ISO (blue) and MT8 (violet) mice received control diets while MAL (green) and EED (red) mice were provided low protein/fat diets. EED and MT8 mice were colonized with CUMT8 *E. coli.*

(B) Percent weight gain during EED protocol. Dotted vertical lines represent days when CUMT8 *E. coli* was orally gavaged. Data shown are representative of three independent experiments (n = 4). Data points represent mean ± SEM. Statistics calculated from weights at day 28.

(C–G) show analyses from day 28 of the EED protocol. Data points represent a single mouse.

(C) Tail lengths. Data shown are one representative example of three independent experiments.

(D) Representative Hematoxylin and Eosin staining of ileal sections. Representative of two separate experiments.

(E) Histological scoring of (D). Pooled from two independent experiments (n = 3/experiment).

(F) Measurement of intestinal permeability by quantification of serum FITC Dextran (4kDA) concentration 4 h after oral gavage. Data are pooled from two independent experiments (n = 3–4/experiment).

(G) Level of CUMT8 *E. coli* in ileal samples from day 23 and day 28 of the EED protocol. Genomic DNA was isolated from ileal contents, and the abundance of CUMT8 was measured by qPCR and compared against a standard curve. Dotted lines represent limit of detection. Data are pooled from two separate experiments (n = 3–4/experiment). Graphs show the mean ± SEM. Statistics calculated by one-way ANOVA (*$p \leq 0.05$; **$p \leq 0.01$; ***$p \leq 0.001$; ****$p \leq 0.0001$).

adherent-invasive *E. coli* "2A" that can attach to the mouse intestine (Molloy et al., 2013; Viladomiu et al., 2021). These experiments showed that the non-adherent ECMB *E. coli* isolate, while colonizing in similar amounts compared to CUMT8 *E. coli* did not induce stunting, while colonization with the adherent 2A isolate reduced growth to a comparable degree as CUMT8 (Figures S1D–S1F). Conversely, gavage of CUMT8 *E. coli* alone had no obvious long-term effects on the mice fed a diet with standard amounts of fat and protein (Figures 1B–1F). We hypothesized that this might be due to differences in the colonization efficiency of CUMT8 *E. coli* under different diets (Brown et al., 2015). Quantification of CUMT8 *E. coli* from ileal and fecal samples of mice fed different diets revealed that malnourishment was necessary for colonization, as mice on the high protein/high fat diet (MT8) displayed only low-level CUMT8 colonization that dissipated quickly (Figure 1G; Figure S1G). In contrast, mice on the low protein/low fat diet (EED) had >10-fold more CUMT8 *E. coli* compared to controls 2 days after CUMT8 gavage, and many animals maintained colonized status for a week or more (Figure 1G; Figure S1G). Therefore, a diet low in protein and fat sets the stage for EED-like disease by directly limiting host growth and allowing for greater levels of colonization with adherent/invasive *E. coli* and thereby intestinal inflammation.

EED induces tissue-specific failure of oral vaccination

In humans, EED is hypothesized to suppress the efficacy of oral vaccines (Bhattacharjee and Hand, 2018; Naylor et al., 2015). To evaluate oral vaccine responses in the murine EED model, we vaccinated mice with an attenuated LT derived from enterotoxigenic *E. coli* (ETEC). This attenuated LT, called double-mutant LT (dmLT) carries two mutations that prevent diarrhea induction by inhibiting host protease-mediated cleavage of the toxin from the plasma membrane and by reducing activation of adenylate cyclase (Clements and Norton, 2018). Despite reduced toxicity, dmLT maintains its immunogenicity as an oral vaccine and generates a robust mixed Th1/Th17 $CD4^+$ T cell and anti-LT IgA B

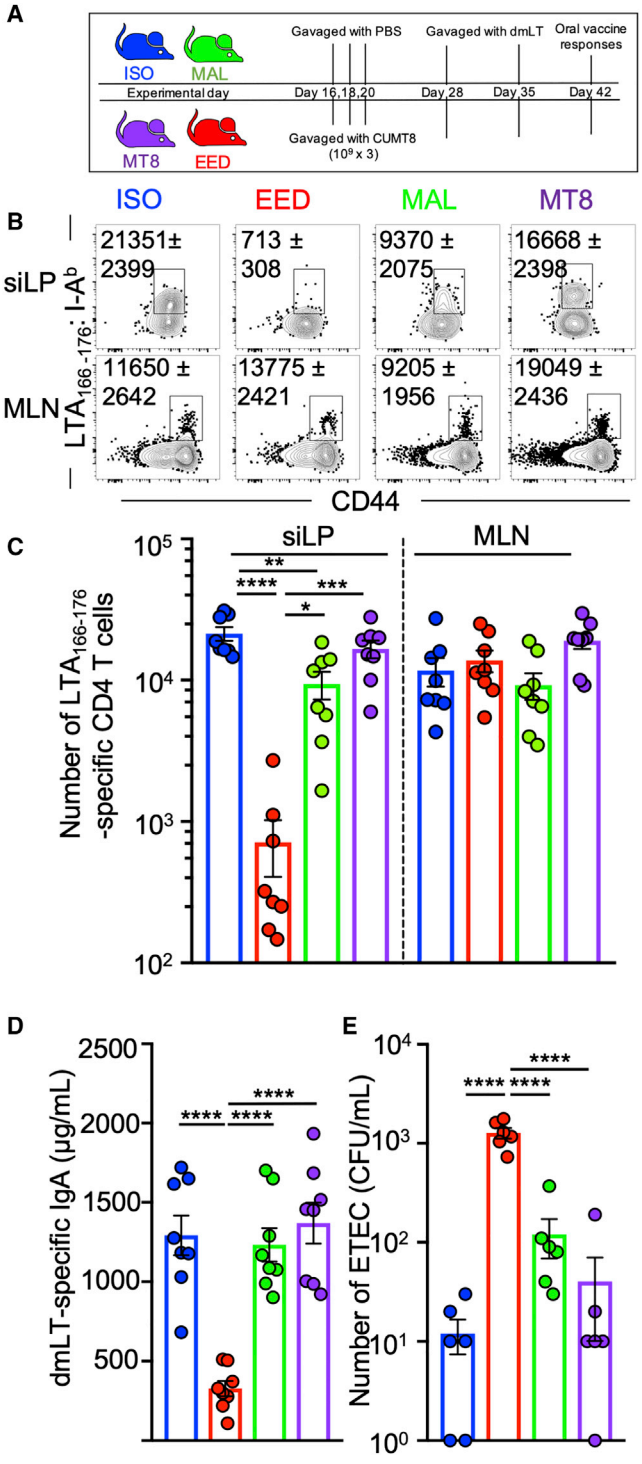

Figure 2. EED induces tissue-specific oral vaccine failure

(A) Schematic of the EED protocol and oral vaccination regime.

(B) Representative flow cytometric plots showing $LT_{166-176}$:I-A^b specific $CD4^+$ T cells from the siLP and MLN, 14 days after primary vaccination with dmLT (day 42). Cells gated: Live, $Lineage^-$, $CD90^+$, $CD3^+$, $CD8b^-$, $CD4^+$. Numbers on plots denote the mean number of cells and SEM, respectively. Data are representative examples of three independent experiments.

(C) Quantification (B). Data are pooled from three independent experiments (n = 2–3/experiment).

(D) Concentration of LT-specific IgA in the small intestine (from PBS lavage) of mice from (C).

(E) Mice in the EED protocol were vaccinated with dmLT as shown in (A). After vaccination (day 42 or 45) mice were colonized with ETEC H10407 ($Kana^R$), and a day later numbers of bacterial colony-forming units (CFU) counted on LB/Kanamycin plates. Data are pooled from two separate experiments (n = 3/experiment).

(C–E) Data points represent a single mouse. Graphs show the mean ± SEM. Statistics calculated by one-way ANOVA (*p ≤ 0.05; **p ≤ 0.01; ***p ≤ 0.001; ****p ≤ 0.0001).

cell response that is dependent upon immune cell activation in the draining mesenteric lymph nodes (MLNs) (Fonseca et al., 2015; Leach et al., 2012). Critically, vaccination of mice with dmLT leads to a $CD4^+$ T cell-dependent protection against intestinal colonization with LT-expressing ETEC (Figure S2A) (Roy et al., 2011).

To test oral vaccine efficacy in our EED model, mice were primed and boosted with dmLT via oral gavage at the end of the EED protocol (Figure 2A) (Hall et al., 2011a). Major histocompatibility complex (MHC) class II tetramers loaded with an epitope from the A-subunit of LT ($LTA_{166-176}$; LT-specific) were used to magnetically isolate and analyze antigen-specific $CD4^+$ T cells from the small intestinal lamina propria (siLP), PPs, and MLNs (Figures 2B and 2C; Figure S2B) (Moon et al., 2009; Pepper et al., 2010). While LT-specific $CD4^+$ T cell responses did not vary across groups in the MLNs and PPs, siLP anti-LT $CD4^+$ T cell responses were almost undetectable in EED mice (>18-fold lower compared to ISO controls), indicating that the vaccine-specific T cells accumulated in the secondary lymphoid tissue but not at the gut mucosa (Figures 2B and 2C; Figure S2B). EED mice also had lower levels of intestinally secreted dmLT-specific immunoglobulin A (IgA) compared to controls, indicating that intestinal IgA^+ B cell responses to oral vaccination were also affected (Figure 2D). Vaccinated EED mice were also incapable of controlling ETEC colonization compared to controls (Figure 2E). In addition, mice fed a low protein/fat MAL diet but orally gavaged with the sessile *E. coli* isolate ECMB (that is insufficient to induce EED) had normal siLP LT-specific $CD4^+$ T cell responses (Figures S1E, S1F, and S2C). Taken together, in a model of EED we have shown that oral vaccines were capable of priming $CD4^+$ T cell responses in the lymph nodes, but vaccine-specific $CD4^+$ T cells fail to accumulate in the small intestine. This suggests that oral vaccine failure in EED might be due to inhibition of intestine-resident T and B cell responses.

EED-associated shifts in the intestinal microbiota are necessary for oral vaccine failure

The intestinal microbiota of children suffering from EED is characterized by overgrowth by *Enterobacteriaceae* and an overrepresentation of bacteria typical to the oropharyngeal cavity (Blanton et al., 2016; Chen et al., 2020; Kau et al., 2015; Vonaesch et al., 2018). In a healthy gut, *Enterobacteriaceae* colonization is controlled by the resident microbiota (Buffie and Pamer, 2013). We wanted to measure whether the increased efficiency of CUMT8 *E.coli* colonization in mice fed a low protein/fat diet was associated with shifts in the intestinal microbiota. To equalize the initial microbiota, mice in these experiments were purchased from a single source and assorted into singly housed cages to avoid "cage-mate" effects on the microbiota.

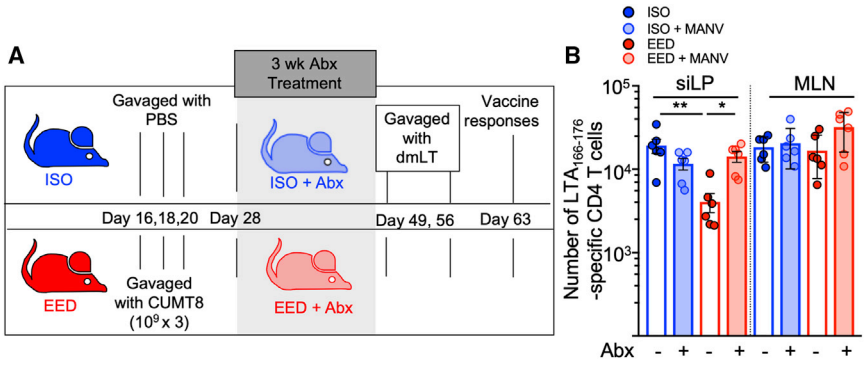

Figure 3. EED-associated shifts in the intestinal microbiome are necessary for oral vaccine failure

(A) Schematic of EED protocol, antibiotic treatment, and vaccination regime. Mice on ISO or EED protocols were treated with antibiotics for three weeks, ending on day 49 when they are orally vaccinated.

(B) Numbers of $LTA_{166-176}$:I-A^b specific $CD4^+$ T cells isolated from the siLP and MLN of mice vaccinated after 3 weeks of treatment with (shaded bars) or without (clear bars) antibiotics. Data points represent a single mouse. Data are pooled from two independent experiments (n = 3/experiment). Graphs show the mean ± SEM. Statistics calculated by one-way ANOVA (*$p \leq 0.05$; **$p \leq 0.01$).

Longitudinal analysis of the fecal microbiota (16S rRNA amplicon sequencing) from our four cohorts revealed that the primary shift was driven by diet, as mice on the low protein/fat diet (MAL: green and EED: red) largely clustered away from mice fed the isocaloric diet (ISO: blue and MT8: purple), highlighting the effect of this diet on the microbiota (Figures S3A and S3B). As mice progressed through the protocol, principal coordinates analysis (PCoA) of the fecal microbiome did not differentiate later fecal sampling time points (experimental day 23 and day 28), indicating the dominance of diet over CUMT8 colonization in determining the structure of the colonic microbiome in these experiments (Figures S3A and S3B). Intestinal inflammation in EED is centered on the ileum, and despite heterogeneity associated with singly housed mice, comparison of the ileal microbiota of ISO and EED mice at day 28 revealed larger differences than for the colonic microbiome (Figures S3C–S3F). In the ileum, the microbiome did not indicate groupings according to diet as MAL and EED were not associated by PCoA, perhaps indicating a dominant role for EED-driven inflammation at this site (Figures S3C–S3E). In concert with human and animal model studies on EED, we observed an increase in *Enterobacteriaceae* and bacteria more commonly associated with the mouth microbiome (*Moraxacellaceae, Veillonellaceae*) among mice with EED (Figure S3F) (Vonaesch et al., 2018). Therefore, we observe that induction of EED in our murine model is associated with diet and inflammation-dependent shifts in the intestinal microbiota.

We next sought to determine if EED-associated changes in the intestinal microbiota were necessary for the reduction in oral vaccine efficacy. To test this question, we treated the EED mice or ISO mice with a broad-spectrum antibiotic cocktail (metronidazole, ampicillin, neomycin, and vancomycin; MANV) to ablate the intestinal microbiota after disease initiation (Figure 3A) (Rakoff-Nahoum et al., 2004). To limit the size of these experiments, we tested only the ISO and EED groups, which show the largest difference in oral vaccine responses. We hypothesized that ablation of the microbiota might reset local immunity and the response to oral vaccination with dmLT. Comparison of the anti-dmLT $CD4^+$ T cell response after 3 weeks of treatment with antibiotics revealed no difference between mice with EED and ISO controls due to an increase in dmLT-specific T cell responses in antibiotic-treated EED mice (Figure 3B). In these experiments, anti-dmLT $CD4^+$ T cell responses in non-antibiotic treated EED mice were not as strongly inhibited, perhaps indicating that the mice began to recover approximately 1 month post-colonization with CUMT8 *E. coli* (Figure 3B). Thus, our EED model exhibits shifts in the composition of the microbiota characteristic of humans with EED, and these shifts are required to maintain EED-associated deficits in the $CD4^+$ T cell response to oral vaccination (Vonaesch et al., 2018).

EED-induced Treg cells are necessary for intestinal oral vaccine failure

The intestine-specific block in oral vaccine responses in the EED mice suggested that the intestinal immune microenvironment may be altered. Therefore, we evaluated the immune cells of the siLP in EED mice and controls. We have previously demonstrated that infection-induced damage to the lymphatics inhibited the traffic of intestinal $CD103^+$ dendritic cells (DCs) to the draining MLNs and induced large shifts in intestinal immune cell populations (Fonseca et al., 2015). In contrast, here we saw no statistically significant differences in the relative abundance of any of the three DC subsets in the MLN, which was consistent with normal activation of LT-specific $CD4^+$ T cells in the MLNs. However, we did observe an increase of $CD11B^+$ $CD103^+$ DCs in the siLP (Figures S4A–S4C). Since the defect in vaccine-specific $CD4^+$ T cells was focused on the small intestine, we next examined major immune populations of the siLP and saw no differences in the proportions of major innate immune cells, B cells, or T cells (Figures S4D–S4I). Children with EED have increased levels of $CD3^+CD25^+$ T cells in their intestine, consistent with an increased number of $FOXP3^+$ Treg cells (Campbell et al., 2003). In accord with human EED phenotypes, mice with EED were found to have an increased number and frequency of Treg cells in their siLP, compared to ISO controls (Figure 4A). In contrast, MLN Treg cell percentages and numbers were invariant across all groups (Figures 4A and 4B). Thus, the abundance of Treg cells at the time of oral vaccination inversely correlated with the accumulation of LT-specific $CD4^+$ T cells at that site. To test the hypothesis that EED-induced Treg cells inhibited oral vaccine responses, EED was induced in $Foxp3^{DTR\text{-}GFP}$ mice, where injection with diphtheria toxin (DT) specifically and transiently ablates $FOXP3^+$ Treg cells (Figure 4C; Figure S4J) (Kim et al., 2007). To target EED-induced Treg cells, DT was administered only for the week post-CUMT8 colonization but prior to vaccination with dmLT (Figure 4C). Treg cell depletion in EED mice completely

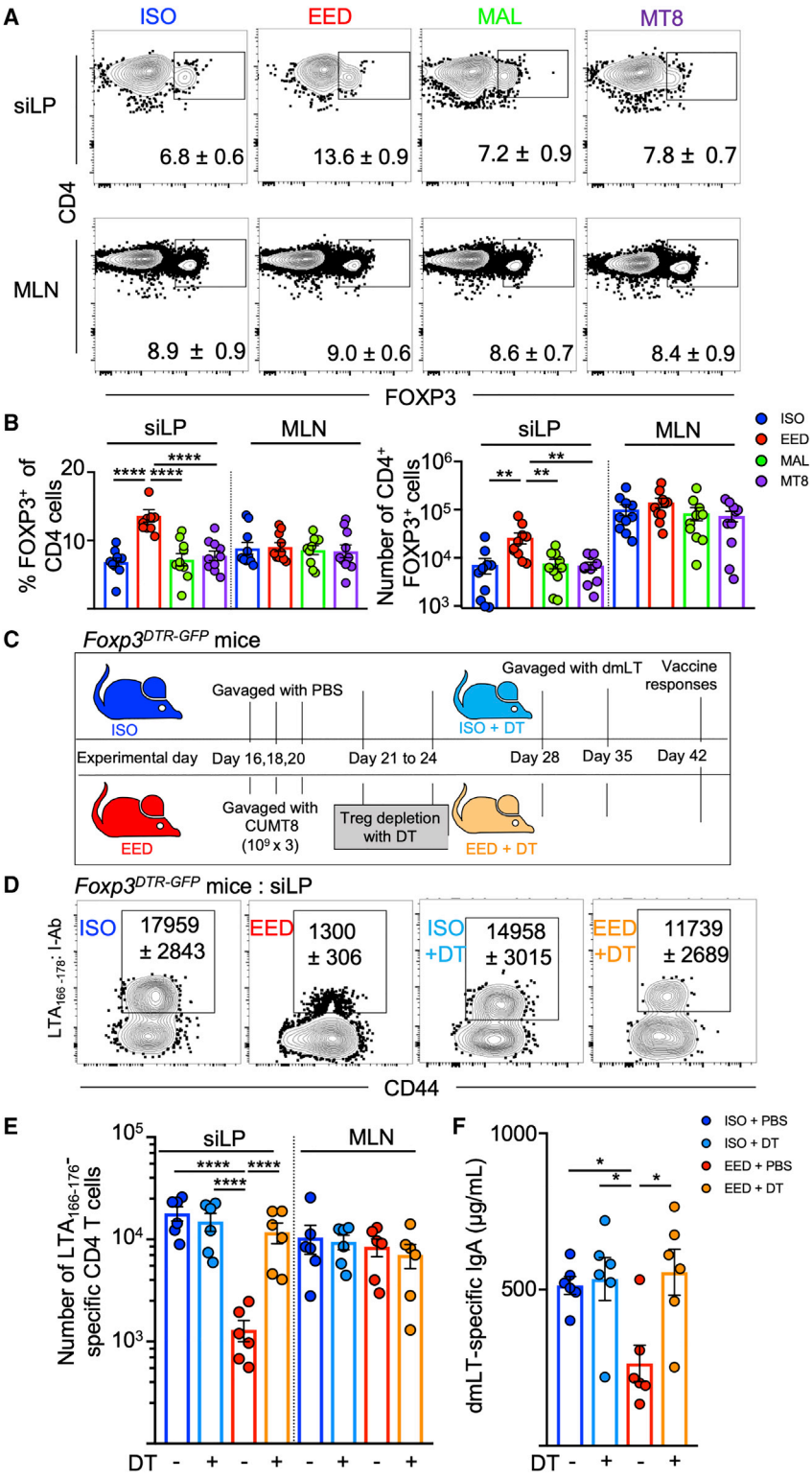

Figure 4. EED-induced Treg cells are necessary for intestinal oral vaccine failure

(A and B) Mice were placed on the ISO, EED, MAL, or MT8 protocols as shown in Figure 1A and sacrificed on day 28.

(A) Representative flow cytometric plots showing percent FOXP3$^+$ CD4$^+$ T cells from the siLP and MLN, as indicated. Gated: Live, CD90$^+$, TCRb$^+$, CD8b$^-$, CD4$^+$. Numbers on plots denote mean and SEM, respectively. Data are representative of three independent experiments (n = 3/experiment).

(B) Percent (left) and numbers (right) of CD4$^+$FOXP3$^+$ T cells from siLP and MLNs from (A). Data are pooled from three experiments.

(C) Schematic of mouse Treg cell depletion experiments using the ISO or EED protocol, *Foxp3*$^{DTR\text{-}GFP}$ mice, and treatment with Diphtheria toxin (C–F).

(D) Representative flow cytometric plots of LTA$_{166–176}$:I-A^b specific CD4$^+$ T cells following oral vaccination of *Foxp3*$^{DTR\text{-}GFP}$ mice with dmLT as in Figure 2. Mice were treated with DT as indicated. Numbers on plots denote the mean number of cells and SEM, respectively. Data shown are representative of two independent experiments (n = 3/experiment).

(E) Number of LTA$_{166\text{-}176}$:I-A^b specific CD4$^+$ T cells calculated from (D). Shown are two pooled experiments.

(F) Concentration of LT-specific IgA in the small intestine (from PBS lavage) from (E).

Data points represent a single mouse. Graphs show the mean ± SEM. Statistics calculated by one-way ANOVA (*p ≤ 0.05; **p ≤ 0.01; ***p ≤ 0.001; ****p ≤ 0.0001).

restored LT-specific CD4$^+$ T cell responses and anti-dmLT IgA responses, while PBS-treated *Foxp3*$^{DTR\text{-}GFP}$ mice still maintained an impairment in these responses (Figures 4D–4F). Therefore, oral vaccine failure in our EED mouse model requires a local increase in small intestinal Treg cells.

EED induces intestinal RORγT-expressing Treg cells that potently suppress CD4$^+$ T cell responses

Given that siLP Treg cells were necessary for the EED-mediated inhibition of oral vaccination, we wanted to determine whether EED-associated intestinal Treg cells were functionally distinct. We found that Treg cells from EED mice expressed higher levels of the proliferation marker Ki67 than ISO mice, potentially accounting for their increased number (Figures 5A and 5B). A critical function of Treg cells is suppression of the clonal expansion of helper T cells. We quantified the suppression capacities of intestinal Treg cells from mice with EED using a microsuppression assay. Treg cells isolated from the siLP of EED mice had greater suppressive potential than the same cells isolated from ISO controls (Figure 5C). Despite their increased functionality, phenotypic characterization of siLP Treg cells from EED mice revealed no statistically significant differences in characteristic Treg proteins such as FOXP3, CD25, CTLA-4, and interleukin-10 (IL-10) (Figures S5A–S5D). However, flow cytometric analysis indicated that siLP Treg cells from EED mice

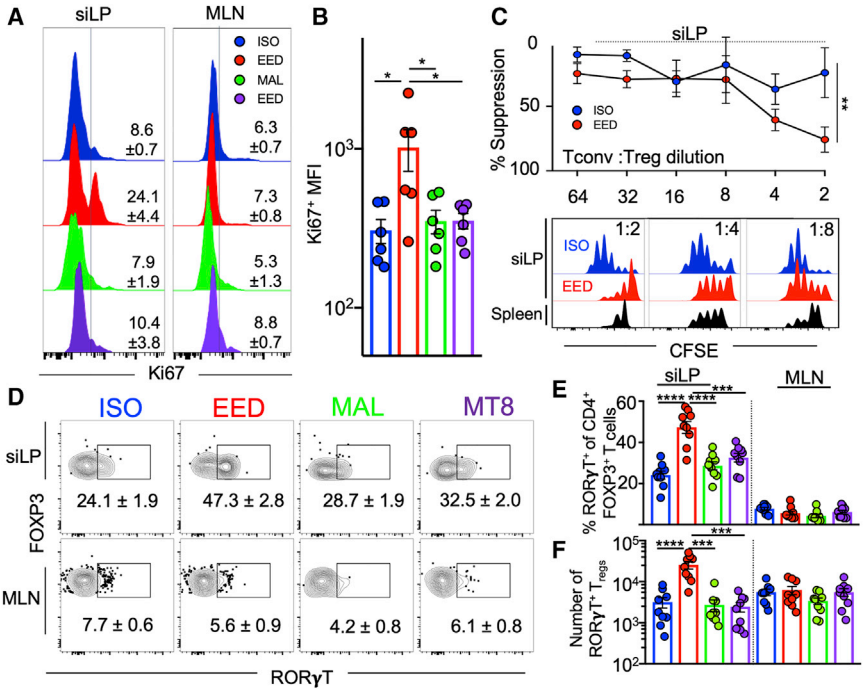

Figure 5. EED induces intestinal RORγT-expressing Treg cells that potently suppress CD4⁺ T cell responses

Mice were placed on the EED protocol as shown in Figure 1A and sacrificed on day 28

(A) Flow cytometric histograms showing percent Ki67 expression in FOXP3⁺CD4⁺ Treg cells from the siLP. Numbers on plots denote mean and SEM, respectively. Data shown are representative of two separate experiments (n = 3/experiment).

(B) Mean fluorescence intensity (MFI) of Ki67 expression from (A). Data are pooled from two experiments.

(C) Percent suppression of naive CD4⁺ T cell proliferation by siLP Treg cells from EED mice or ISO controls (n = 5). Top is line graph showing relative suppression at different cellular concentrations. Bottom is representative histograms of Tconv CFSE dilution. Black histograms represent suppression by splenic Treg cells from ISO mice. Data points and error bars represent mean and SEM respectively (**p ≤ 0.01; 2-way ANOVA). Data shown are representative of two independent experiments where siLP Treg cells were sorted from 4 EED and 4 ISO mice.

(D) Representative flow cytometric contour plots of RORγT expression on siLP (top) and MLN (bottom) FOXP3⁺ CD4⁺ Treg cells. Numbers on plots denote the mean percent positive and SEM, respectively. Data shown are representative of three independent experiments (n = 3/experiment).

(E) Percent and (F) numbers of FOXP3⁺ CD4⁺ Treg cells from (D) that express RORγT. Data are pooled from three separate experiments.

(B, E, and F) Data points represent a single mouse. Graphs show the mean ± SEM. Statistics for (B), (E), and (F) were calculated by one-way ANOVA (*p < 0.05; **p < 0.01; ***p < 0.001; ****p ≤ 0.0001).

had increased expression of CD39 and CD73 (Figure S5E), a pair of ectonucleotidases that dephosphorylate extracellular ATP sequentially to adenosine and are associated with increased suppressive function in Treg cells (Deaglio et al., 2007).

The microbiota and, in particular, intestinal bacteria that adhere to the intestinal epithelium are associated with the induction of intestinal Treg cells that express the transcription factor RORγT (Kim et al., 2016; Ohnmacht et al., 2015; Sefik et al., 2015; Xu et al., 2018). Analysis of EED mice and controls revealed that siLP Treg cells from EED mice showed a distinct increase in RORγT⁺ Treg cells that did not extend to Treg cells isolated from the MLNs (Figures 5D–5F). The development of RORγT⁺ Treg cells in the colon requires the presence of specific types of intestinal bacteria (Abdel-Gadir et al., 2019; Sefik et al., 2015; Song et al., 2020; Xu et al., 2018). Therefore, we sought to analyze the effects of the EED microbiota on siLP Treg cells. Antibiotic depletion of the microbiota for 3 weeks eliminated the EED-induced increase RORγT⁺ Treg cells in the small intestine (Figure S5F), which corresponds well with the finding that ablation of the microbiota can largely restore the ability of mice with EED to induce intestinal immune responses to oral vaccination (Figure 3B). Intestinal RORγT⁺ Treg cells are also supported by the expression of inflammatory cytokines, such as IL-6 and IL-23, and the presence of the vitamin A metabolite, retinoic acid (Ohnmacht et al., 2015; Yan et al., 2021). Analysis of the cytokine milieu of the small intestine of EED mice and ISO controls did not reveal differences in IL-6 and IL-23 but did show increases of IL-2 and IL-10, two cytokines important for Treg cell homeostasis in the intestine (Murai et al., 2009; Zhou et al., 2019) (Figure S5G). The production of retinoic acid (RA) from retinaldehyde is catalyzed by an aldehyde dehydrogenase: RALDH2, which is expressed in migratory DCs found in the siLP and MLN (Hall et al., 2011b). Flow cytometric analysis showed that aldehyde dehydrogenase (ALDH) enzymatic activity was specifically increased among DCs in the siLP but not DCs isolated from the MLNs (Figures S5H and S5I). Most ALDH activity was found among CD103⁺ DCs, though an increase in activity was found in both intestinal CD103⁺ and CD103⁻ DCs (Figures S5H and S5I). Taken altogether, we have shown that EED is associated with the specific expansion of small intestinal RORγT⁺CD39⁺CD73⁺ Treg cells endowed with increased regulatory function. Further, the accumulation of RORγT⁺ Treg cells in the small intestine requires the presence of the intestinal microbiota and is associated with the distinct upregulation of retinoic acid production capability of intestinal DCs.

RORγT-expression in Treg cells is necessary to inhibit vaccine-specific CD4⁺ T cell responses and EED-associated stunting

RORγT⁺ Treg cells can suppress inflammation in animal models of colonic pathology (Ohnmacht et al., 2015; Sefik et al., 2015), but their role in the small intestine and specifically in oral vaccine responses is not known. Therefore, we bred *Foxp3*$^{Cre\ ERT2}$ *Rorc*$^{fl/fl}$ mice (FOXP3$^{RORγT+/-}$) where the expression of RORγT can be specifically extinguished in FOXP3⁺ Treg cells via the administration of tamoxifen (FOXP3$^{RORγT-}$) (Figure 6A; Figure S6A) (Rubtsov et al., 2010). We gavaged mice with tamoxifen to excise the *Rorc* gene in developing Treg cells starting from 5 days before CUMT8 *E. coli* gavage to the end of the EED protocol. When immunized with dmLT, tamoxifen-treated

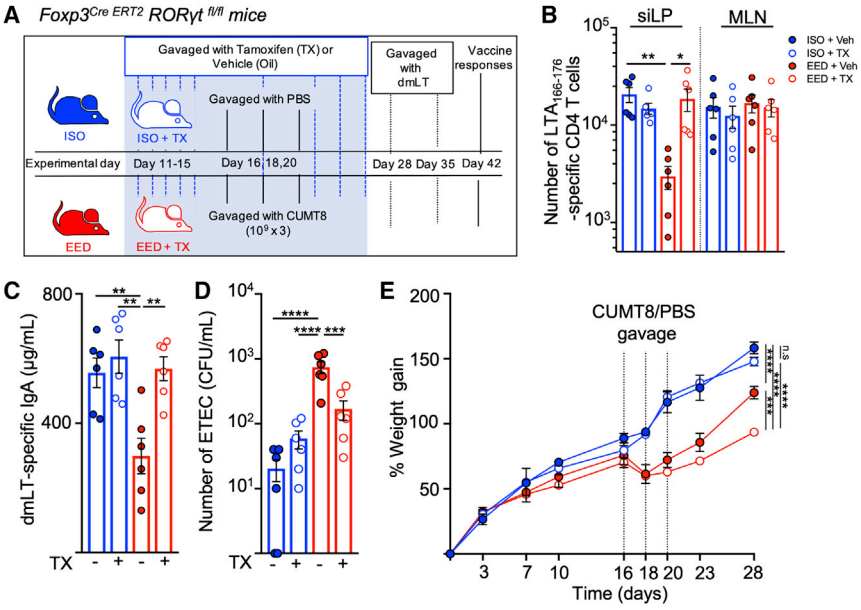

Figure 6. Blocking RORγT induction in EED induced Treg cells restores oral vaccine responses

(A) Schematic of ISO or EED protocols, tamoxifen (TX) or vehicle (Veh; corn oil) treatment for RORγT deletion and oral vaccination and in *Foxp3*$^{Cre\ ERT2}$ *Rorc*$^{fl/fl}$ mice (FOXP3$^{RORgT+/-}$).

(B–E) Data from mice which were treated with tamoxifen (FOXP3^{RORgT-}) are represented in open circles whereas data from vehicle treated controls (FOXP3^{RORgT+}) are in closed circles.

(B) Numbers of LT$_{166-176}$:I-A^{b} specific CD4^{+} T cells isolated from the siLP and MLNs following oral vaccination with dmLT (as in Figure 2A) of *Foxp3*$^{Cre\ ERT2}$ *Rorc*$^{fl/fl}$ with and without tamoxifen treatment. Data are pooled from two separate experiments (n = 3/experiment).

(C) Concentration of LT-specific IgA in the small intestine (from PBS lavage) of *Foxp3*$^{Cre\ ERT2}$ *Rorc*$^{fl/fl}$ mice from mice from (B).

(D) *Foxp3*$^{Cre\ ERT2}$ *Rorc*$^{fl/fl}$ mice in the EED protocol were vaccinated with dmLT, with and without tamoxifen treatment as shown in (A). After vaccination (day 42 or 45) mice were colonized with ETEC H10407 (Kana^{R}) and a day later numbers of bacterial CFU counted on LB/Kanamycin plates. Data are pooled from two separate experiments (n = 3/experiment).

(E) Percent weight gain during EED establishment in FOXP3$^{Cre\ ERT2}$ Rorc $^{fl/fl}$ mice with and without tamoxifen treatment. Dotted lined represent days when CUMT8 *E. coli* was orally gavaged. Data shown are representative of two separate experiments (n = 3-4/experiment). Statistics calculated from weights at day 28.

Graphs show the mean ± SEM. Data points represent a single mouse. Statistics calculated by one-way ANOVA (*p ≤ 0.05; **p ≤ 0.01)

FOXP3$^{RORγT-}$ mice showed completely restored LT-specific CD4^{+} T cell populations in the siLP and had normal production of anti-dmLT IgA, while vehicle-gavaged controls (FOXP3$^{RORγt+}$) still showed reduced responses (Figures 6B and 6C). Critically, deletion of the Rorc gene from Treg cells also restored the ability of mice on the EED protocol to develop oral vaccine-mediated protective immunity, as vaccinated FOXP3$^{RORγT-}$ mice showed a reduction in ETEC colonization compared to vehicle-treated EED mice (Figure 6D). Treg-specific ablation of RORγT had an effect on the total number and frequency of siLP Treg cells in EED mice, indicating that RORγT may play a role in the accumulation and survival of FOXP3^{+} Treg cells in the intestine (Figures S6B and S6C).

Since we treated mice with tamoxifen during EED induction, we were able to determine if RORγT^{+} Treg cells are important for controlling any of the symptoms of EED. Interestingly, FOXP3$^{RORγt-}$ EED mice were more stunted than RORγT^{+} Treg sufficient EED controls (FOXP3$^{RORγt+}$) under the same protocol and gained minimal weight after colonization with CUMT8 *E. coli* (Figure 6E; Figure S6D**)**. Thus, RORγT expression in Treg cells is not only necessary to inhibit the accumulation of vaccine-specific T cells in the small intestine but is also important for reducing stunting associated with EED. We hypothesize that the accumulation of RORγT^{+} Treg cells in the intestine of EED may result from an effort to alleviate chronic intestinal inflammation in the small intestine and that the localized failure of vaccine-specific T cell responses at this site develops as a side effect of a tissue-specific immunoregulation.

DISCUSSION

We have developed a murine model of EED that mimics several aspects of human disease, including a reduction in immunity conferred by oral vaccination. Areas of the world where EED is endemic exhibit a lack of efficacy of oral vaccines, which is tragic since these communities would probably benefit most from effective mucosal immune protection (Grassly et al., 2009; Levine, 2010). There are a variety of factors other than EED that contribute to the failure of oral vaccines in resource-poor countries, including extended breast feeding (which may contain vaccine inhibitory IgA and milk oligosaccharides), increased exposure to pollution, micronutrient deficiency, and pathogen heterogeneity (Burr et al., 2020; Moon et al., 2010; Santos and Hoshino, 2005). We found that independent of other factors, EED is sufficient to inhibit siLP CD4^{+} T cell responses and IgA production, indicating that EED is an important contributor to failure of oral vaccines in resource poor countries (Di Luccia et al., 2020).

Adherent-invasive *E. coli* were first described in patients with Crohn's disease where they contribute to pathology but are not sufficient to induce disease since they are common in the general population (Barnich and Darfeuille-Michaud, 2007). It is likely that our ancestors were commonly colonized with bacteria that attach to and irritate the intestinal epithelium and engender CD4^{+} T cell responses. We propose that EED is inducing local immune suppression, mediated by RORγt^{+} Treg cells, to limit inflammatory intestinal damage. In this model, systemic immunity is left intact to guard against more invasive organisms. However, a side effect of this EED-induced intestinal immune shutdown is the loss of efficient tissue responses to oral vaccines. We hypothesize that this represents an evolutionary mechanism to prevent chronic inflammation in the small intestine, such as inflammatory bowel disease in the face of constant colonization with intestinally adherent bacteria.

Most research on oral vaccines has focused on antibodies. However, there is a growing interest in the potential of

intestinal-resident CD4$^+$ T cells in mediating protection via the rapid production of cytokines, such as IL-17A and IL-22, that can activate defense mechanisms in the intestinal epithelium (Cao et al., 2012; Omenetti et al., 2019; Schreiber et al., 2015). A recent trial using oral dmLT in combination with live-attenuated enterotoxigenic *E. coli* vaccine revealed significant protection that was not correlated to antigen-specific IgA or IgG, leaving the possibility of a T cell-mediated mechanism (Clements and Norton, 2018; Harro et al., 2019). CD4$^+$ T cells also support the differentiation and development of IgA$^+$ plasma B cells in PPs (Bemark et al., 2016; Lycke and Bemark, 2017), but, surprisingly, we saw very few LT-specific T cells in the PPs in our studies, and they did not vary according to nutritional/EED status. After activation in the PPs, IgA$^+$ plasma cells traffic to siLP where they will reside long-term (Lycke and Bemark, 2017). Perhaps siLP CD4$^+$ T cells assist B cells in the small intestinal lamina propria or, alternatively, the inflammatory and nutrient-deficient environment of the EED intestine may inhibit IgA-producing B cells independently of T cell help. Future studies on LT-specific B cells in EED will be necessary to elucidate this point.

In our model of EED, we correlated oral vaccine failure with an increased presence of RORγT$^+$ Treg cells within the small intestine but not in the draining MLN tissue. This is consistent with human studies where children suffering from EED have increased CD3$^+$CD25$^+$ cells in their intestine (Campbell et al., 2003). Most previous descriptions of RORγT$^+$ Treg cells have focused on the colon, where these cells are dependent upon the production of bile acid metabolites and specific members of the microbiota (Sefik et al., 2015; Song et al., 2020; Xu et al., 2018). The majority of bile acids are recycled by the ileum so they could also be important in inducing RORγT$^+$ Treg cells in the small intestine (Ridlon et al., 2006). The intestinal metabolite profile of the small intestine is substantially different between EED mice and controls, with bile acid metabolism/synthesis among the largest differences (Brown et al., 2015). Alternatively, RORγT$^+$ Treg cells are also observed in lung tissue, where bile acids are not present at high levels, implying that there may be multiple pathways that drive this subset (Lochner et al., 2008). Retinoic acid production, presumably mediated by intestine-derived DCs, is also required for colonic RORγT$^+$ Treg cells, and here we found an intestine-specific increase in ALDH activity among those DCs. While induction of Treg cells specific to intestinally derived antigens occurs in the gut-draining mesenteric lymph nodes, RORγT$^+$ Treg cells are rare at this site, implying that like RORγT-expressing Th17 cells, further differentiation of these cells occurs upon arrival in the intestine (Sano et al., 2015). Indeed, IL-6 expressed by enteric nerves is critical for the development of colonic RORγT$^+$ Treg cells, and we hypothesize that the increase in intestinal RA production has a similar effect, acting on Treg cells after they arrive in the intestine (Yan et al., 2021). Antigen-specific RORγT$^+$ Treg cells are also induced by colonization of the cecum and colon with *Helicobacter hepaticus* (Xu et al., 2018). It is not clear whether the RORγT$^+$ Treg cells induced by EED are specific to CUMT8 *E. coli* but both *H. hepaticus* and CUMT8 *E. coli* share the ability to adhere to the surface of the intestine (Dogan et al., 2014; Fox et al., 1994). Adherence to the gut lining is likely critical for the induction of RORγT$^+$ Treg cells (Kim et al., 2018), as seen by the lack of oral vaccine failure in malnourished mice that were given ECMB, a non-adherent strain of *E. coli*. Further experimentation will be needed to identify whether epithelium-adherent bacteria are required to activate RORγT$^+$ Treg cells in the small intestine.

The molecular mechanism by which RORγT$^+$ Treg cells limit the accumulation of LT-specific CD4$^+$ T cells is not clear. Our hypothesis is that RORγT$^+$ Treg cells are blocking local antigen presentation and cytokine signals that are necessary for secondary proliferation once LT-specific T cells arrive in the intestine (Sano et al., 2015). The function that RORγT performs as a transcription factor in Treg cells is also not clear at this point, but our results showed that RORγT expression may be important for Treg proliferation and survival in the intestine. Loss of RORγT expression from Treg cells does not lead to spontaneous intestinal inflammation but instead is critical to limiting inflammation once it is induced (Boehm et al., 2012; Ohnmacht et al., 2015; Sefik et al., 2015). For example, RORγT$^+$ Treg cells were superior to RORγT$^-$ Treg cells at suppressing inflammation in a model of T cell transfer colitis (Yang et al., 2016). In concert, our results show that RORγt$^+$ Treg cells reduce EED-associated stunting. Since the primary function of the gut is to absorb nutrients, we hypothesize that RORγt$^+$ Treg cells prioritize epithelial health and absorption and that the block in immune responses is a by-product of the necessity to regulate damaging inflammation. Patients suffering from EED can take years to re-establish full intestinal functionality, and it will be important to determine whether, once established, intestinal resident immune cells maintain the disease state long after the inciting conditions have subsided (Gerson et al., 1971; Lindenbaum et al., 1972). In the future, as we develop a deeper knowledge of the intestinal immune defects in EED, we hope that this information can be incorporated into treatment plans and oral vaccine formulations so we can break the chain of malnutrition and infection that underlies this disease.

Limitations of the study

Our study tests an animal model of a complex human disease. While our model recapitulates many aspects of human EED, there are undoubtedly many ways that mouse physiology differs from humans, some of which may be important to this model. While we feel that our EED model will be useful for the research community to test hypotheses mechanistically, it will be important to determine these differences. For example, our model relies on adherent/invasive *E. coli* (AIEC), and while *E. coli* is increased in children with EED, AIEC may be irrelevant to human disease. Our study uncovered a failure of vaccine-specific CD4$^+$ T cells to accumulate in the intestine due to local increases in Treg cells; however, limitations on how many tissues we could analyze per experiment prevented us from determining whether EED was driving vaccine-specific T cells to a different tissue. In addition, we relied on flow cytometric measurements of antigen-specific CD4$^+$ T cells isolated from enzymatically degraded tissue. A more comprehensive view of the oral vaccine-specific CD4$^+$ T cell response would be provided by microscopy, but this will necessitate a shift away from tetramer-based identification of T cells, which is technically challenging in fixed tissue. Finally, while we saw a drop in LT-specific IgA, we did not measure a difference in total IgA or IgA-bound bacteria in the small intestine. We have hypothesized that EED is primarily affecting T cell dependent IgA$^+$ B cell differentiation and that the level of T independent IgA remains intact. A more in-depth study of LT-specific B cells and potentially T-B interaction in the PPs of EED mice will be required to answer these questions.

STAR★METHODS

Detailed methods are provided in the online version of this paper and include the following:

- KEY RESOURCES TABLE
- RESOURCE AVAILABILITY
  - Lead contact
  - Materials availability
  - Data and code availability
- EXPERIMENTAL MODEL AND SUBJECT DETAILS
  - Mice
  - Cell culture and microbial strains
- METHOD DETAILS
  - EED induction
  - Histological analysis of terminal ileums
  - FITC–dextran assay
  - LT-specific tetramer production
  - Oral vaccination and isolation of vaccine specific cells
  - *In vivo* ETEC challenge
  - Antibiotic treatment
  - qRT-PCR analysis
  - 16S rRNA amplicon analysis of relative bacterial abundance
  - Flow cytometry
  - Suppression assay
  - Anti-dmLT ELISA
  - Luminex assays
  - ALDH activity assay
  - Diphtheria toxin (DT) and tamoxifen (TX) administration
- QUANTIFICATION AND STATISTICAL ANALYSIS

SUPPLEMENTAL INFORMATION

Supplemental information can be found online at https://doi.org/10.1016/j.immuni.2021.07.005.

ACKNOWLEDGMENTS

This work was supported by the National Institutes of Health (R21AI142051; T.W.H., NIAID division of Intramural Research; Y.B., FAPESP-JP 2015/25364-0; D.M.F.), the R.K. Mellon Institute for Pediatric Research (T.W.H.), and the UPMC Children's Hospital of Pittsburgh RAC award (A.B.). A.E.O. is supported by a Damon Runyon Cancer Research Foundation Postdoctoral Fellowship (2360-19), and A.H.P.B. is supported by a NIH T32 (T32AI089443). The authors would like to thank J. Michel and A. Styche for assistance with cell sorting, the UPMC Children's Hospital of Pittsburgh Histology core for the preparation of tissue slides, and the University of Pittsburgh Division of Laboratory Animal Research. We would also like to thank D. Vignali (Foxp3$^{eGFP\text{-}Cre\text{-}ERT2}$), K. Simpson (CUMT8 *E. coli*), R. Longman (2A *E. coli*), J. Fleckenstein (ETEC), and J. Williams (Foxp3$^{DTR\text{-}GFP}$) for sharing critical reagents, and M. Pepper and M. Jenkins for assistance with making and using MHC class II tetramer reagents. We would like to thank the University of Pittsburgh Center for Research Computing for resources and assistance with microbiome sequence analysis. We would like to thank the members of the Hand, Belkaid, Poholek, and Canna labs for discussion and critical reading of the manuscript. The graphical abstract was produced using BioRender.

AUTHOR CONTRIBUTIONS

A.B., A.E.O., and T.W.H. designed the experiments; A.B., A.H.P.B., A.E.O., J.T.T., D.Y., and B.R.H. carried out the experiments; A.B., A.H.P.B., A.E.O., and T.W.H. analyzed the data; J.L.L., S.P.S., J.A.H., O.J.H., D.M.F., E.B.N., Y.B., and T.W.H. contributed to the development of reagents (MHC class II tetramers) and models to study anti-LT responses *in vivo*; E.B.N. provided recombinant LT and dmLT for these studies; A.B. and T.W.H. wrote the manuscript.

DECLARATION OF INTERESTS

The authors declare no competing interests.

Received: May 18, 2020
Revised: April 21, 2021
Accepted: July 9, 2021
Published: August 3, 2021

REFERENCES

Abdel-Gadir, A., Stephen-Victor, E., Gerber, G.K., Noval Rivas, M., Wang, S., Harb, H., Wang, L., Li, N., Crestani, E., Spielman, S., et al. (2019). Microbiota therapy acts via a regulatory T cell MyD88/RORγt pathway to suppress food allergy. Nat. Med. *25*, 1164–1174.

Ansaldo, E., Slayden, L.C., Ching, K.L., Koch, M.A., Wolf, N.K., Plichta, D.R., Brown, E.M., Graham, D.B., Xavier, R.J., Moon, J.J., and Barton, G.M. (2019). *Akkermansia muciniphila* induces intestinal adaptive immune responses during homeostasis. Science *364*, 1179–1184.

Barnich, N., and Darfeuille-Michaud, A. (2007). Adherent-invasive Escherichia coli and Crohn's disease. Curr. Opin. Gastroenterol. *23*, 16–20.

Bemark, M., Hazanov, H., Strömberg, A., Komban, R., Holmqvist, J., Köster, S., Mattsson, J., Sikora, P., Mehr, R., and Lycke, N.Y. (2016). Limited clonal relatedness between gut IgA plasma cells and memory B cells after oral immunization. Nat. Commun. *7*, 12698.

Bhattacharjee, A., and Hand, T.W. (2018). Role of nutrition, infection, and the microbiota in the efficacy of oral vaccines. Clin. Sci. (Lond.) *132*, 1169–1177.

Blanton, L.V., Barratt, M.J., Charbonneau, M.R., Ahmed, T., and Gordon, J.I. (2016). Childhood undernutrition, the gut microbiota, and microbiota-directed therapeutics. Science *352*, 1533.

Boehm, F., Martin, M., Kesselring, R., Schiechl, G., Geissler, E.K., Schlitt, H.J., and Fichtner-Feigl, S. (2012). Deletion of Foxp3+ regulatory T cells in genetically targeted mice supports development of intestinal inflammation. BMC Gastroenterol. *12*, 97.

Bolyen, E., Rideout, J.R., Dillon, M.R., Bokulich, N.A., Abnet, C.C., Al-Ghalith, G.A., Alexander, H., Alm, E.J., Arumugam, M., Asnicar, F., et al. (2019). Reproducible, interactive, scalable and extensible microbiome data science using QIIME 2. Nat. Biotechnol. *37*, 852–857.

Brown, E.M., Wlodarska, M., Willing, B.P., Vonaesch, P., Han, J., Reynolds, L.A., Arrieta, M.C., Uhrig, M., Scholz, R., Partida, O., et al. (2015). Diet and specific microbial exposure trigger features of environmental enteropathy in a novel murine model. Nat. Commun. *6*, 7806.

Buffie, C.G., and Pamer, E.G. (2013). Microbiota-mediated colonization resistance against intestinal pathogens. Nat. Rev. Immunol. *13*, 790–801.

Burr, A.H.P., Bhattacharjee, A., and Hand, T.W. (2020). Nutritional Modulation of the Microbiome and Immune Response. J. Immunol. *205*, 1479–1487.

Callahan, B.J., McMurdie, P.J., Rosen, M.J., Han, A.W., Johnson, A.J., and Holmes, S.P. (2016). DADA2: High-resolution sample inference from Illumina amplicon data. Nat. Methods *13*, 581–583.

Campbell, D.I., Elia, M., and Lunn, P.G. (2003). Growth faltering in rural Gambian infants is associated with impaired small intestinal barrier function, leading to endotoxemia and systemic inflammation. J. Nutr. *133*, 1332–1338.

Cao, A.T., Yao, S., Gong, B., Elson, C.O., and Cong, Y. (2012). Th17 cells upregulate polymeric Ig receptor and intestinal IgA and contribute to intestinal homeostasis. J. Immunol. *189*, 4666–4673.

Carmody, R.N., Gerber, G.K., Luevano, J.M., Jr., Gatti, D.M., Somes, L., Svenson, K.L., and Turnbaugh, P.J. (2015). Diet dominates host genotype in shaping the murine gut microbiota. Cell Host Microbe *17*, 72–84.

Chai, J.N., Peng, Y., Rengarajan, S., Solomon, B.D., Ai, T.L., Shen, Z., Perry, J.S.A., Knoop, K.A., Tanoue, T., Narushima, S., et al. (2017). *Helicobacter*

species are potent drivers of colonic T cell responses in homeostasis and inflammation. Sci. Immunol. *2*. https://doi.org/10.1126/sciimmunol.aal5068.

Chen, R.Y., Kung, V.L., Das, S., Hossain, M.S., Hibberd, M.C., Guruge, J., Mahfuz, M., Begum, S.M.K.N., Rahman, M.M., Fahim, S.M., et al. (2020). Duodenal Microbiota in Stunted Undernourished Children with Enteropathy. N. Engl. J. Med. *383*, 321–333.

Chiaranunt, P., Tometich, J.T., Ji, J., and Hand, T.W. (2018). T Cell Proliferation and Colitis Are Initiated by Defined Intestinal Microbes. J. Immunol. *201*, 243–250.

Choi, G.B., Yim, Y.S., Wong, H., Kim, S., Kim, H., Kim, S.V., Hoeffer, C.A., Littman, D.R., and Huh, J.R. (2016). The maternal interleukin-17a pathway in mice promotes autism-like phenotypes in offspring. Science *351*, 933–939.

Clements, J.D., and Norton, E.B. (2018). The Mucosal Vaccine Adjuvant LT(R192G/L211A) or dmLT. MSphere *3*, e00215–e00218.

Cong, Y., Feng, T., Fujihashi, K., Schoeb, T.R., and Elson, C.O. (2009). A dominant, coordinated T regulatory cell-IgA response to the intestinal microbiota. Proc. Natl. Acad. Sci. USA *106*, 19256–19261.

Cotillard, A., Kennedy, S.P., Kong, L.C., Prifti, E., Pons, N., Le Chatelier, E., Almeida, M., Quinquis, B., Levenez, F., Galleron, N., et al.; ANR MicroObes consortium (2013). Dietary intervention impact on gut microbial gene richness. Nature *500*, 585–588.

Craven, M., Egan, C.E., Dowd, S.E., McDonough, S.P., Dogan, B., Denkers, E.Y., Bowman, D., Scherl, E.J., and Simpson, K.W. (2012). Inflammation drives dysbiosis and bacterial invasion in murine models of ileal Crohn's disease. PLoS ONE *7*, e41594.

Deaglio, S., Dwyer, K.M., Gao, W., Friedman, D., Usheva, A., Erat, A., Chen, J.F., Enjyoji, K., Linden, J., Oukka, M., et al. (2007). Adenosine generation catalyzed by CD39 and CD73 expressed on regulatory T cells mediates immune suppression. J. Exp. Med. *204*, 1257–1265.

Di Luccia, B., Ahern, P.P., Griffin, N.W., Cheng, J., Guruge, J.L., Byrne, A.E., Rodionov, D.A., Leyn, S.A., Osterman, A.L., Ahmed, T., et al. (2020). Combined Prebiotic and Microbial Intervention Improves Oral Cholera Vaccination Responses in a Mouse Model of Childhood Undernutrition. Cell Host Microbe *27*, 899–908.

Dickson, B.C., Streutker, C.J., and Chetty, R. (2006). Coeliac disease: an update for pathologists. J. Clin. Pathol. *59*, 1008–1016.

Dogan, B., Suzuki, H., Herlekar, D., Sartor, R.B., Campbell, B.J., Roberts, C.L., Stewart, K., Scherl, E.J., Araz, Y., Bitar, P.P., et al. (2014). Inflammation-associated adherent-invasive Escherichia coli are enriched in pathways for use of propanediol and iron and M-cell translocation. Inflamm. Bowel Dis. *20*, 1919–1932.

Fonseca, D.M., Hand, T.W., Han, S.J., Gerner, M.Y., Glatman Zaretsky, A., Byrd, A.L., Harrison, O.J., Ortiz, A.M., Quinones, M., Trinchieri, G., et al. (2015). Microbiota-Dependent Sequelae of Acute Infection Compromise Tissue-Specific Immunity. Cell *163*, 354–366.

Fox, J.G., Dewhirst, F.E., Tully, J.G., Paster, B.J., Yan, L., Taylor, N.S., Collins, M.J., Jr., Gorelick, P.L., and Ward, J.M. (1994). Helicobacter hepaticus sp. nov., a microaerophilic bacterium isolated from livers and intestinal mucosal scrapings from mice. J. Clin. Microbiol. *32*, 1238–1245.

Gerson, C.D., Kent, T.H., Saha, J.R., Siddiqi, N., and Lindenbaum, J. (1971). Recovery of small-intestinal structure and function after residence in the tropics. II. Studies in Indians and Pakistanis living in New York City. Ann. Intern. Med. *75*, 41–48.

Grassly, N.C., Jafari, H., Bahl, S., Durrani, S., Wenger, J., Sutter, R.W., and Aylward, R.B. (2009). Mucosal immunity after vaccination with monovalent and trivalent oral poliovirus vaccine in India. J. Infect. Dis. *200*, 794–801.

Gribonika, I., Eliasson, D.G., Chandode, R.K., Schön, K., Strömberg, A., Bemark, M., and Lycke, N.Y. (2019). Class-switch recombination to IgA in the Peyer's patches requires natural thymus-derived Tregs and appears to be antigen independent. Mucosal Immunol. *12*, 1268–1279.

Haberman, Y., Iqbal, N.T., Ghandikota, S., Mallawaarachchi, I., Tzipi Braun, Dexheimer, P.J., Rahman, N., Hadar, R., Sadiq, K., Ahmad, Z., et al. (2021). Mucosal Genomics Implicate Lymphocyte Activation and Lipid Metabolism in Refractory Environmental Enteric Dysfunction. Gastroenterology *160*, 2055–2071.

Hall, J.A., Cannons, J.L., Grainger, J.R., Dos Santos, L.M., Hand, T.W., Naik, S., Wohlfert, E.A., Chou, D.B., Oldenhove, G., Robinson, M., et al. (2011a). Essential role for retinoic acid in the promotion of CD4(+) T cell effector responses via retinoic acid receptor alpha. Immunity *34*, 435–447.

Hall, J.A., Grainger, J.R., Spencer, S.P., and Belkaid, Y. (2011b). The role of retinoic acid in tolerance and immunity. Immunity *35*, 13–22.

Hand, T.W. (2016). The Role of the Microbiota in Shaping Infectious Immunity. Trends Immunol. *37*, 647–658.

Hand, T.W., Dos Santos, L.M., Bouladoux, N., Molloy, M.J., Pagán, A.J., Pepper, M., Maynard, C.L., Elson, C.O., 3rd, and Belkaid, Y. (2012). Acute gastrointestinal infection induces long-lived microbiota-specific T cell responses. Science *337*, 1553–1556.

Hand, T.W., Vujkovic-Cvijin, I., Ridaura, V.K., and Belkaid, Y. (2016). Linking the Microbiota, Chronic Disease, and the Immune System. Trends Endocrinol. Metab. *27*, 831–843.

Harro, C., Louis Bourgeois, A., Sack, D., Walker, R., DeNearing, B., Brubaker, J., Maier, N., Fix, A., Dally, L., Chakraborty, S., et al. (2019). Live attenuated enterotoxigenic Escherichia coli (ETEC) vaccine with dmLT adjuvant protects human volunteers against virulent experimental ETEC challenge. Vaccine *37*, 1978–1986.

Henao-Mejia, J., Elinav, E., Jin, C., Hao, L., Mehal, W.Z., Strowig, T., Thaiss, C.A., Kau, A.L., Eisenbarth, S.C., Jurczak, M.J., et al. (2012). Inflammasome-mediated dysbiosis regulates progression of NAFLD and obesity. Nature *482*, 179–185.

Honda, K., and Littman, D.R. (2016). The microbiota in adaptive immune homeostasis and disease. Nature *535*, 75–84.

Katoh, K., Misawa, K., Kuma, K., and Miyata, T. (2002). MAFFT: a novel method for rapid multiple sequence alignment based on fast Fourier transform. Nucleic Acids Res. *30*, 3059–3066.

Kau, A.L., Planer, J.D., Liu, J., Rao, S., Yatsunenko, T., Trehan, I., Manary, M.J., Liu, T.C., Stappenbeck, T.S., Maleta, K.M., et al. (2015). Functional characterization of IgA-targeted bacterial taxa from undernourished Malawian children that produce diet-dependent enteropathy. Sci. Transl. Med. *7*, 276ra24.

Kawamoto, S., Maruya, M., Kato, L.M., Suda, W., Atarashi, K., Doi, Y., Tsutsui, Y., Qin, H., Honda, K., Okada, T., et al. (2014). Foxp3(+) T cells regulate immunoglobulin a selection and facilitate diversification of bacterial species responsible for immune homeostasis. Immunity *41*, 152–165.

Keusch, G.T., Denno, D.M., Black, R.E., Duggan, C., Guerrant, R.L., Lavery, J.V., Nataro, J.P., Rosenberg, I.H., Ryan, E.T., Tarr, P.I., et al. (2014). Environmental enteric dysfunction: pathogenesis, diagnosis, and clinical consequences. Clin. Infect. Dis. *59* (*Suppl 4*), S207–S212.

Kim, J.M., Rasmussen, J.P., and Rudensky, A.Y. (2007). Regulatory T cells prevent catastrophic autoimmunity throughout the lifespan of mice. Nat. Immunol. *8*, 191–197.

Kim, K.S., Hong, S.W., Han, D., Yi, J., Jung, J., Yang, B.G., Lee, J.Y., Lee, M., and Surh, C.D. (2016). Dietary antigens limit mucosal immunity by inducing regulatory T cells in the small intestine. Science *351*, 858–863.

Kim, M., Galan, C., Hill, A.A., Wu, W.J., Fehlner-Peach, H., Song, H.W., Schady, D., Bettini, M.L., Simpson, K.W., Longman, R.S., et al. (2018). Critical Role for the Microbiota in CX3CR1(+) Intestinal Mononuclear Phagocyte Regulation of Intestinal T Cell Responses. Immunity *49*, 151–163.

Korpe, P.S., and Petri, W.A., Jr. (2012). Environmental enteropathy: critical implications of a poorly understood condition. Trends Mol. Med. *18*, 328–336.

Kozono, H., White, J., Clements, J., Marrack, P., and Kappler, J. (1994). Production of soluble MHC class II proteins with covalently bound single peptides. Nature *369*, 151–154.

Leach, S., Clements, J.D., Kaim, J., and Lundgren, A. (2012). The adjuvant double mutant Escherichia coli heat labile toxin enhances IL-17A production in human T cells specific for bacterial vaccine antigens. PLoS ONE *7*, e51718.

Leung, J.M., Davenport, M., Wolff, M.J., Wiens, K.E., Abidi, W.M., Poles, M.A., Cho, I., Ullman, T., Mayer, L., and Loke, P. (2014). IL-22-producing CD4+ cells are depleted in actively inflamed colitis tissue. Mucosal Immunol. *7*, 124–133.

Levine, M.M. (2010). Immunogenicity and efficacy of oral vaccines in developing countries: lessons from a live cholera vaccine. BMC Biol. *8*, 129.

Lindenbaum, J., Harmon, J.W., and Gerson, C.D. (1972). Subclinical malabsorption in developing countries. Am. J. Clin. Nutr. *25*, 1056–1061.

Lochner, M., Peduto, L., Cherrier, M., Sawa, S., Langa, F., Varona, R., Riethmacher, D., Si-Tahar, M., Di Santo, J.P., and Eberl, G. (2008). In vivo equilibrium of proinflammatory IL-17+ and regulatory IL-10+ Foxp3+ RORgamma t+ T cells. J. Exp. Med. *205*, 1381–1393.

Lycke, N.Y., and Bemark, M. (2017). The regulation of gut mucosal IgA B-cell responses: recent developments. Mucosal Immunol. *10*, 1361–1374.

McDonald, D., Price, M.N., Goodrich, J., Nawrocki, E.P., DeSantis, T.Z., Probst, A., Andersen, G.L., Knight, R., and Hugenholtz, P. (2012). An improved Greengenes taxonomy with explicit ranks for ecological and evolutionary analyses of bacteria and archaea. ISME J. *6*, 610–618.

McMurchy, A.N., and Levings, M.K. (2012). Suppression assays with human T regulatory cells: a technical guide. Eur. J. Immunol. *42*, 27–34.

Molloy, M.J., Grainger, J.R., Bouladoux, N., Hand, T.W., Koo, L.Y., Naik, S., Quinones, M., Dzutsev, A.K., Gao, J.L., Trinchieri, G., et al. (2013). Intraluminal containment of commensal outgrowth in the gut during infection-induced dysbiosis. Cell Host Microbe *14*, 318–328.

Moon, J.J., Chu, H.H., Pepper, M., McSorley, S.J., Jameson, S.C., Kedl, R.M., and Jenkins, M.K. (2007). Naive CD4(+) T cell frequency varies for different epitopes and predicts repertoire diversity and response magnitude. Immunity *27*, 203–213.

Moon, J.J., Chu, H.H., Hataye, J., Pagán, A.J., Pepper, M., McLachlan, J.B., Zell, T., and Jenkins, M.K. (2009). Tracking epitope-specific T cells. Nat. Protoc. *4*, 565–581.

Moon, S.S., Wang, Y., Shane, A.L., Nguyen, T., Ray, P., Dennehy, P., Baek, L.J., Parashar, U., Glass, R.I., and Jiang, B. (2010). Inhibitory effect of breast milk on infectivity of live oral rotavirus vaccines. Pediatr. Infect. Dis. J. *29*, 919–923.

Murai, M., Turovskaya, O., Kim, G., Madan, R., Karp, C.L., Cheroutre, H., and Kronenberg, M. (2009). Interleukin 10 acts on regulatory T cells to maintain expression of the transcription factor Foxp3 and suppressive function in mice with colitis. Nat. Immunol. *10*, 1178–1184.

Naylor, C., Lu, M., Haque, R., Mondal, D., Buonomo, E., Nayak, U., Mychaleckyj, J.C., Kirkpatrick, B., Colgate, R., Carmolli, M., et al.; PROVIDE study teams (2015). Environmental Enteropathy, Oral Vaccine Failure and Growth Faltering in Infants in Bangladesh. EBioMedicine *2*, 1759–1766.

Norton, E.B., Lawson, L.B., Freytag, L.C., and Clements, J.D. (2011). Characterization of a mutant Escherichia coli heat-labile toxin, LT(R192G/L211A), as a safe and effective oral adjuvant. Clin. Vaccine Immunol. *18*, 546–551.

Ohnmacht, C., Park, J.H., Cording, S., Wing, J.B., Atarashi, K., Obata, Y., Gaboriau-Routhiau, V., Marques, R., Dulauroy, S., Fedoseeva, M., et al. (2015). MUCOSAL IMMUNOLOGY. The microbiota regulates type 2 immunity through RORγt$^+$ T cells. Science *349*, 989–993.

Omenetti, S., Bussi, C., Metidji, A., Iseppon, A., Lee, S., Tolaini, M., Li, Y., Kelly, G., Chakravarty, P., Shoaie, S., et al. (2019). The Intestine Harbors Functionally Distinct Homeostatic Tissue-Resident and Inflammatory Th17 Cells. Immunity *51*, 77–89.

Pasetti, M.F., Simon, J.K., Sztein, M.B., and Levine, M.M. (2011). Immunology of gut mucosal vaccines. Immunol. Rev. *239*, 125–148.

Pepper, M., Linehan, J.L., Pagán, A.J., Zell, T., Dileepan, T., Cleary, P.P., and Jenkins, M.K. (2010). Different routes of bacterial infection induce long-lived TH1 memory cells and short-lived TH17 cells. Nat. Immunol. *11*, 83–89.

Price, M.N., Dehal, P.S., and Arkin, A.P. (2010). FastTree 2–approximately maximum-likelihood trees for large alignments. PLoS ONE *5*, e9490.

Rakoff-Nahoum, S., Paglino, J., Eslami-Varzaneh, F., Edberg, S., and Medzhitov, R. (2004). Recognition of commensal microflora by toll-like receptors is required for intestinal homeostasis. Cell *118*, 229–241.

Ridaura, V.K., Faith, J.J., Rey, F.E., Cheng, J., Duncan, A.E., Kau, A.L., Griffin, N.W., Lombard, V., Henrissat, B., Bain, J.R., et al. (2013). Gut microbiota from twins discordant for obesity modulate metabolism in mice. Science *341*, 1241214.

Ridlon, J.M., Kang, D.J., and Hylemon, P.B. (2006). Bile salt biotransformations by human intestinal bacteria. J. Lipid Res. *47*, 241–259.

Rolhion, N., and Darfeuille-Michaud, A. (2007). Adherent-invasive Escherichia coli in inflammatory bowel disease. Inflamm. Bowel Dis. *13*, 1277–1283.

Roy, K., Hamilton, D.J., Munson, G.P., and Fleckenstein, J.M. (2011). Outer membrane vesicles induce immune responses to virulence proteins and protect against colonization by enterotoxigenic Escherichia coli. Clin. Vaccine Immunol. *18*, 1803–1808.

Rubtsov, Y.P., Niec, R.E., Josefowicz, S., Li, L., Darce, J., Mathis, D., Benoist, C., and Rudensky, A.Y. (2010). Stability of the regulatory T cell lineage in vivo. Science *329*, 1667–1671.

Sano, T., Huang, W., Hall, J.A., Yang, Y., Chen, A., Gavzy, S.J., Lee, J.Y., Ziel, J.W., Miraldi, E.R., Domingos, A.I., et al. (2015). An IL-23R/IL-22 Circuit Regulates Epithelial Serum Amyloid A to Promote Local Effector Th17 Responses. Cell *163*, 381–393.

Santos, N., and Hoshino, Y. (2005). Global distribution of rotavirus serotypes/genotypes and its implication for the development and implementation of an effective rotavirus vaccine. Rev. Med. Virol. *15*, 29–56.

Schreiber, F., Arasteh, J.M., and Lawley, T.D. (2015). Pathogen Resistance Mediated by IL-22 Signaling at the Epithelial-Microbiota Interface. J. Mol. Biol. *427*, 3676–3682.

Sefik, E., Geva-Zatorsky, N., Oh, S., Konnikova, L., Zemmour, D., McGuire, A.M., Burzyn, D., Ortiz-Lopez, A., Lobera, M., Yang, J., et al. (2015). MUCOSAL IMMUNOLOGY. Individual intestinal symbionts induce a distinct population of RORγ$^+$ regulatory T cells. Science *349*, 993–997.

Segata, N., Izard, J., Waldron, L., Gevers, D., Miropolsky, L., Garrett, W.S., and Huttenhower, C. (2011). Metagenomic biomarker discovery and explanation. Genome Biol. *12*, R60.

Shaikh, H., Lynch, J., Kim, J., and Excler, J.L. (2020). Current and future cholera vaccines. Vaccine *38* (*Suppl 1*), A118–A126.

Song, X., Sun, X., Oh, S.F., Wu, M., Zhang, Y., Zheng, W., Geva-Zatorsky, N., Jupp, R., Mathis, D., Benoist, C., and Kasper, D.L. (2020). Microbial bile acid metabolites modulate gut RORγ$^+$ regulatory T cell homeostasis. Nature *577*, 410–415.

Tsuji, M., Komatsu, N., Kawamoto, S., Suzuki, K., Kanagawa, O., Honjo, T., Hori, S., and Fagarasan, S. (2009). Preferential generation of follicular B helper T cells from Foxp3+ T cells in gut Peyer's patches. Science *323*, 1488–1492.

Turnbaugh, P.J., Ley, R.E., Mahowald, M.A., Magrini, V., Mardis, E.R., and Gordon, J.I. (2006). An obesity-associated gut microbiome with increased capacity for energy harvest. Nature *444*, 1027–1031.

Turnis, M.E., Sawant, D.V., Szymczak-Workman, A.L., Andrews, L.P., Delgoffe, G.M., Yano, H., Beres, A.J., Vogel, P., Workman, C.J., and Vignali, D.A. (2016). Interleukin-35 Limits Anti-Tumor Immunity. Immunity *44*, 316–329.

Vela Ramirez, J.E., Sharpe, L.A., and Peppas, N.A. (2017). Current state and challenges in developing oral vaccines. Adv. Drug Deliv. Rev. *114*, 116–131.

Viladomiu, M., Metz, M.L., Lima, S.F., Jin, W.B., Chou, L., Guo, C.J., Diehl, G.E., Simpson, K.W., Scherl, E.J., and Longman, R.S.; JRI Live Cell Bank (2021). Adherent-invasive E. coli metabolism of propanediol in Crohn's disease regulates phagocytes to drive intestinal inflammation. Cell Host Microbe *29*, 607–619.

Vonaesch, P., Morien, E., Andrianonimiadana, L., Sanke, H., Mbecko, J.R., Huus, K.E., Naharimanananirina, T., Gondje, B.P., Nigatoloum, S.N., Vondo, S.S., et al.; Afribiota Investigators (2018). Stunted childhood growth is associated with decompartmentalization of the gastrointestinal tract and overgrowth of oropharyngeal taxa. Proc. Natl. Acad. Sci. USA *115*, E8489–E8498.

Wadolkowski, E.A., Laux, D.C., and Cohen, P.S. (1988). Colonization of the streptomycin-treated mouse large intestine by a human fecal Escherichia coli strain: role of growth in mucus. Infect. Immun. *56*, 1030–1035.

Watanabe, K., and Petri, W.A., Jr. (2016). Environmental Enteropathy: Elusive but Significant Subclinical Abnormalities in Developing Countries. EBioMedicine *10*, 25–32.

Weiss, J.M., Bilate, A.M., Gobert, M., Ding, Y., Curotto de Lafaille, M.A., Parkhurst, C.N., Xiong, H., Dolpady, J., Frey, A.B., Ruocco, M.G., et al. (2012). Neuropilin 1 is expressed on thymus-derived natural regulatory T cells, but not mucosa-generated induced Foxp3+ T reg cells. J Exp Med *209*, 1723–1742.

Xu, M., Pokrovskii, M., Ding, Y., Yi, R., Au, C., Harrison, O.J., Galan, C., Belkaid, Y., Bonneau, R., and Littman, D.R. (2018). c-MAF-dependent regulatory T cells mediate immunological tolerance to a gut pathobiont. Nature *554*, 373–377.

Yan, Y., Ramanan, D., Rozenberg, M., McGovern, K., Rastelli, D., Vijaykumar, B., Yaghi, O., Voisin, T., Mosaheb, M., Chiu, I., et al. (2021). Interleukin-6 produced by enteric neurons regulates the number and phenotype of microbe-responsive regulatory T cells in the gut. Immunity *54*, 499–513.

Yang, B.H., Hagemann, S., Mamareli, P., Lauer, U., Hoffmann, U., Beckstette, M., Föhse, L., Prinz, I., Pezoldt, J., Suerbaum, S., et al. (2016). Foxp3(+) T cells expressing RORγt represent a stable regulatory T-cell effector lineage with enhanced suppressive capacity during intestinal inflammation. Mucosal Immunol. *9*, 444–457.

Zhao, Q., Harbour, S.N., Kolde, R., Latorre, I.J., Tun, H.M., Schoeb, T.R., Turner, H., Moon, J.J., Khafipour, E., Xavier, R.J., et al. (2017). Selective Induction of Homeostatic Th17 Cells in the Murine Intestine by Cholera Toxin Interacting with the Microbiota. J. Immunol. *199*, 312–322.

Zhou, L., Chu, C., Teng, F., Bessman, N.J., Goc, J., Santosa, E.K., Putzel, G.G., Kabata, H., Kelsen, J.R., Baldassano, R.N., et al. (2019). Innate lymphoid cells support regulatory T cells in the intestine through interleukin-2. Nature *568*, 405–409.

STAR★METHODS

KEY RESOURCES TABLE

REAGENT or RESOURCE	SOURCE	IDENTIFIER
Antibodies		
Mouse Anti-mouse CD45.2 (104), APC-eFluor 780	Invitrogen	Cat#47-0454-82; RRID: AB_1272175; Clone: 104
Rat Anti-Mouse CD90.2 (30-H12), Brilliant Violet 605	BD Biosciences	Cat#740334; RRID: AB_2740067; Clone: 30-H12
Rat Anti-mouse CD3 molecular complex (17A2), PerCP-Cyanine5.5	BD Biosciences	Cat#560527; RRID: AB_1727463; Clone: 17A2
Hamster Anti-mouse TCR beta (H57-597), APC-eFluor 780	Invitrogen	Cat# 47-5961-82; RRID: AB_1272173; H57-597
Rat Anti-Mouse CD4 (RM4-5), Brilliant Violet 786	BD Biosciences	Cat#563727; RRID: AB_2728707; Clone: RM4-5
Rat Anti-mouse CD8b (H35-17.2), PE-Cyanine7	Invitrogen	Cat#25-0083-82; RRID: AB_11218494; Clone H35-17.2
Rat Anti-mouse CD44 (IM7), FITC	BD Biosciences	Cat#553133; RRID: AB_2076224; Clone: IM7
Rat Anti-mouse CD44 (IM7), PerCP-Cyanine5.5	Invitrogen	Cat#45-0441-82; RRID: AB_925746; Clone: IM7
Rat Anti-mouse FOXP3 (FJK-16 s), Alexa Fluor 488	Invitrogen	Cat#53-5773-82; RRID: AB_763537; Clone: FJK-16 s
Rat Anti-mouse FOXP3 (FJK-16 s), eFluor 450	Invitrogen	Cat#48-5773-82; RRID: AB_1518812; Clone: FJK-16 s
Rat Anti-mouse CD304 (Neuropilin-1) (3E12), PE-Cyanine7	Biolegend	Cat#145212; RRID: AB_2562360; Clone: 3E12
Rat Anti-mouse ROR gamma (t) (B2D), PE	Invitrogen	Cat#12-6981-82; RRID: AB_10807092; Clone: B2D
Rat Anti-mouse Ki67 (16A8), FITC	Biolegend	Cat#652410; RRID: AB_2562141; Clone: 16A8
Rat Anti-mouse CD39 (Duha59), PE-Dazzle™ 594	Biolegend	Cat#143812; RRID: AB_2750322; Clone: Duha59
Rat Anti-mouse CD73 (TY/11.8), Alexa Fluor 700	Biolegend	Cat#127230; RRID: AB_2800625; Clone: TY/11.8
Rat Anti-mouse CD11b (M1/70), PE-Cyanine7	Invitrogen	Cat#25-0112-82; RRID: AB_469588; Clone: M1/70
Hamster Anti-mouse CD11c (HL3), PerCP-Cyanine5.5	BD Biosciences	Cat# 560584; RRID: AB_1727422; Clone: HL3
Rat Anti-mouse Ly-6C (HK1.4), eFluor 450	Invitrogen	Cat#48-5932-82; RRID: AB_10805519; Clone: HK1.4
Rat Anti-mouse I-A/I-E (M5/114.15.2), Brilliant Violet 786	BD Biosciences	Cat#742894; RRID: AB_2734759; Clone: M5/114.15.2
Mouse Anti-mouse Cd64 (FcγRI) (X54-5/7.1), Brilliant Violet 605	Biolegend	Cat#139323; RRID: AB_2629778; Clone: X54-5/7.1
Rat Anti-mouse CD170 (Siglec F) (1RNM44N), eFluor 660	Invitrogen	Cat#50-1702-82; RRID: AB_2574187; Clone: 1RNM44N
Rat Anti-mouse Ly-6G (1A8), PE-CF594	BD Biosciences	Cat#562700; RRID: AB_2737730; Clone: 1A8
Rat Anti-mouse CD19 (1D3), PE-CF594	BD Biosciences	Cat#562291; RRID: AB_11154223; Clone: 1D3
Rat Anti-mouse TER-119 (TER-119), PE-eFluor 610	Invitrogen	Cat#61-5921-80; RRID: AB_2574637; Clone: TER-119

(*Continued on next page*)

Continued

REAGENT or RESOURCE	SOURCE	IDENTIFIER
Rat Anti-mouse CD11b (M1/70), PE-CF594	BD Biosciences	Cat#562317; RRID: AB_11154422; Clone: M1/70
Hamster Anti-mouse CD11c (HL3), PE-CF594	BD Biosciences	Cat#562454; RRID: AB_2737617; Clone: HL3
InVivoMAb anti-mouse CD4 (GK1.5)	BioXCell	Cat#BE0003-1; RRID: AB_1107636; Clone: GK1.5
Goat Anti-Mouse IgA-HRP	SouthernBiotech	Cat#1040-05; RRID: AB_2714213
Rat Anti-mouse CD16/32 (93)	Invitrogen	Cat#14-0161-86; RRID: AB_467135; Clone: 93
Bacterial and virus strains		
CUMT8 bacteria	(Craven et al., 2012; Dogan et al., 2014)	N/A
ECMB bacteria	(Molloy et al., 2013)	N/A
E. coli 2A	(Viladomiu et al., 2021)	N/A
ETEC Kana^{Res}(jf876)	(Roy et al., 2011)	N/A
Biological samples		
Stool samples and ileal contents from EED mice	This study	N/A
Chemicals, peptides, and recombinant proteins		
Double mutant Labile Toxin (dmLT) from *E. coli*	Elizabeth Norton (Tulane) (Norton et al., 2011)	N/A
Ionomycin	Millipore Sigma	Cat#I0634; CAS: 56092-82-1
Phorbol 12-myristate 13-acetate	Millipore Sigma	Cat#P8139; CAS: 16561-29-8
Brefeldin A	Invitrogen	Cat#00-4506-51
Fluorescein isothiocyanate–dextran	Millipore Sigma	Cat#FD4; CAS: 60842-46-8
LB Agar Plates, Kanamycin-50	Teknova	Cat#L1025
Metronidazole	Millipore Sigma	Cat#M1547; CAS: 443-48-1
Ampicillin sodium salt	Millipore Sigma	Cat#A0166; CAS: 69-52-3
Neomycin trisulfate salt hydrate	Millipore Sigma	Cat#N6386; CAS: 1405-10-3
Vancomycin hydrochloride	Millipore Sigma	Cat#V1130; CAS: 1404-93-9
Diphtheria Toxin	Millipore Sigma	Cat#D0564; MDL: MFCD00163490
Tamoxifen	Millipore Sigma	Cat#T5648; CAS: 10540-29-1
Corn oil	Millipore Sigma	CAS: 8001-30-7
Fixable Live/Dead Aqua	Invitrogen	Cat#L34966
Saccharin	Acros Organics	Cat#AC149005000
Monomeric Avidin UltraLink™ Resin	Thermo Scientific	Cat#53146
Streptavidin-APC	Prozyme/Agilent	Cat#PJ27S-1
Streptavidin-PE	Prozyme/Agilent	Cat#PJRS25-1
Blasticidin	Invivogen	Cat#ant-bl-1
Critical commercial assays		
FoxP3/Transcription Factor Staining Buffer Set Cat#: 00-5523-00	Invitrogen	Cat#00-5523-00
Intracellular Fixation and and Permeabilization Buffer Set	Thermo Fisher Scientific	Cat#: 88-8824-00
EasySep™ APC Positive Selection Kit II	StemCell Technologies, Inc.	Cat#17681
QIAamp Fast DNA Stool Mini Kit	QIAGEN	Cat#51604
MILLIPLEX MAP Mouse TH17 Magnetic Bead Panel - Immunology Multiplex Assay	Millipore Sigma	Cat#MTH17MAG-47K

(*Continued on next page*)

Continued

REAGENT or RESOURCE	SOURCE	IDENTIFIER
SsoAdvanced Universal SYBR® Green Supermix	Bio-Rad	Cat#1725270
Calcium Phosphate Transfection Kit	Invitrogen	Cat# K278001
His-Tag Purification Kit	Millipore Sigma	Cat#70239-3
Ultra-15 30kDa MWCO Centrifugal Filter Units	Millipore Sigma	Cat#UFC903024
Deposited data		
16S rDNA amplicon sequencing of Stool samples and ileal contents from EED and control mice	This manuscript	Database : PRJNA736663
Experimental models: Cell lines		
Drosophila S2 Cells in Schneider's Medium	GIBCO	Cat#R69007
Experimental models: Organisms/strains		
Specific Pathogen Free C57BL/6NTac mice	Taconic Farms	*MGI:5658006*
Foxp3^{DTR} mice	Jackson Labs (Kim et al., 2007)	JAX stock #016958
Foxp3$^{eGFP\text{-}Cre\text{-}ERT2}$ mice	Jackson Labs (Rubtsov et al., 2010).	JAX stock #016961
Rorγt^{fl} mice	Jackson Labs (Choi et al., 2016; .	JAX stock #008771
Oligonucleotides		
16S primer Fwd 5′-ACTCCTACGGGAGGCAGCAGT-3′	IDT	N/A
16S primer Rev 5′-ATTACCGCGGCTGCTGGC-3′.	IDT	N/A
ECMB OmpL Fwd 5′-TTCGGGTGGTGCAGTGTATC-3′	IDT	N/A
ECMB OmpL Rev 5′-TGCTGCTATTAAAGTCATTTACGC-3′	IDT	N/A
CUMT8 FliC Fwd 5′-CGACAGTGCCGGTATTTGTA-3′	IDT	N/A
CUMT8 FliC Rev 5′-TGAGTACTGCGGATGGTTCA-3′	IDT	N/A
LCN2	QIAGEN	PPMO3770A
Gapdh	QIAGEN	PPM41731A
Recombinant DNA		
Mouse I-Ab alpha chain on pRMHa-3 backbone	Jenkins lab, Moon et al.	N/A
Mouse I-Ab beta chain with LT166-176 peptide DNA sequence on pRMHa-3 backbone	Jenkins lab, Moon et al.	N/A
Software and algorithms		
FlowJo X	BD Biosciences	N/A
FACSDiva	BD Biosciences	N/A
Prism 9	GraphPad	9.02
R Studio	R Studio	N/A
Phyloseq	https://joey711.github.io/phyloseq/	N/A
QIIME 2 2020.2	(Bolyen et al., 2019).	N/A
DADA2	(Callahan et al., 2016)	N/A
mafft	(Katoh et al., 2002)	N/A
fasttree2	(Price et al., 2010)	N/A
Greengenes 13_8 99% OTUs reference sequences	(McDonald et al., 2012)	N/A

(*Continued on next page*)

Continued

REAGENT or RESOURCE	SOURCE	IDENTIFIER
MicrobeR	J Bisanz, 2018 https://www.biorxiv.org/content/10.1101/304840v1	N/A
LEfSe	https://huttenhower.sph.harvard.edu/galaxy/root	N/A
Other		
Low protein/low fat diet (7% protein/7% fat)	Research Diets Brown et al., 2015	D14071001
Isocaloric diet (20% protein/15% fat)	Research Diets Brown et al., 2015	D09051102

RESOURCE AVAILABILITY

Lead contact

Further information and requests for resources and reagents should be directed to and will be fulfilled by the Lead Contact: Timothy Hand (timothy.hand@chp.edu)

Materials availability

- The LT specific MHCII tetramer generated for this study will be available by contacting the Lead Contact.
- The data generated by 16 s sequencing for this study (Database : PRJNA736663) has been deposited to the BioProject database.

Data and code availability

- 16S rDNA amplicon sequencing data from stool samples and ileal contents from mice are publicly available through NCBI under the accession number PRJNA736663.
- This paper does not report original code.
- Any additional information required to reanalyze the data reported in this paper is available from the lead contact upon request.

EXPERIMENTAL MODEL AND SUBJECT DETAILS

Mice

Three-week-old wild type C57BL/6Tac mice (B6 MPF; Taconic) were used for EED establishment and characterization unless otherwise noted. Foxp3$^{DTR\text{-}GFP}$ (*Foxp3*$^{tm3(DTR/GFP)Ayr}$) mice, were the kind gift of John Williams (UPMC Children's Hospital of Pittsburgh) (Kim et al., 2007). Foxp3$^{eGFP\text{-}Cre\text{-}ERT2}$ (*Foxp3* $^{tm9(EGFP/cre/ERT2)Ayr}$) mice were the kind gift of Dario Vignali (University of Pittsburgh) and bred with Rorc$^{fl/fl}$ mice (B6(Cg)-^{Rorctm3Litt}) from Jackson Laboratories (Choi et al., 2016; Rubtsov et al., 2010). Both male and female age-matched mice (three weeks) were used for all experiments. Littermates of the same sex were randomly assigned to experimental groups. All experiments were performed in an American Association for the Accreditation of Laboratory Animal Care-accredited animal facility at the University of Pittsburgh. Mice were weaned onto special diets and kept in specific pathogen-free conditions and housed in accordance with the procedures outlined in the Guide for the Care and Use of Laboratory Animals under an animal study proposal approved by the Institutional Animal Care and Use Committee of the University of Pittsburgh. For 16S rRNA gene sequencing experiments, all animals were singly housed to prevent cage effects of the microbiota.

Cell culture and microbial strains

Drosophila S2 cells were used for tetramer production and were cultured in Schneider's Medium at 28°C before transfection. CUMT8, an autochthonous mouse adherent invasive *E. coli* (Dogan et al., 2014), was provided by Kenneth Simpson (Cornell University, Ithaca, NY; transferred to Univ. of Pittsburgh by MTA). In some experiments, a mouse commensal *E. coli* (ECMB) was used in place of CUMT8 (Molloy et al., 2013) to study the effect of adherence as ECMB lacks a flagellar operon and is non-motile. *E. coli* 2A (Viladomiu et al., 2021; transferred to Univ. of Pittsburgh by MTA), an AIEC isolated from a patient with Crohn's disease was provided by from Randy Longman (NYU School of Medicine, New York,NY). ETEC jf876, a Kanamycin resistant strain derived from ETEC H10407 (Roy et al., 2011) was obtained from James Fleckenstein (Washington University School of Medicine in St. Louis). All bacteria were grown in Luria Broth in 125 mL conical flasks in a 37°C shaker incubator.

METHOD DETAILS

EED induction

Immediately following arrival, mice are placed on one of two special diets (Research Diets); a malnourished low protein/low fat diet (7% protein/7% fat; D14071001)), or a control isocaloric diet (20% protein/15% fat; D09051102) (Brown et al., 2015). Chow was

added bi-weekly to ensure that malnourished mice did not compensate for protein/fat deficiencies in their diet by increasing intake and all mice were provided the same amount of calories each week. Some groups of mice (MT8 and EED) were orally gavaged with $1x10^9$ CUMT8 *E. coli* on experimental days 16, 18 and 20. Mice were weighed biweekly. After 28 days on diets, mice were sacrificed and evaluated for signs of EED. Alternatively, mice were then treated or immunized at experimental day 28.

Histological analysis of terminal ileums

Terminal ileum samples were fixed in formalin, dehydrated and paraffin embedded. Sections of ileum were stained with hematoxylin and eosin stains for morphological analysis and slides were scored using the modified Marsh-Oberhuber classification (Dickson et al., 2006). Scoring was carried out by a student who was blinded to the experimental groups Outline of scoring system: 0 = Pre-infiltrative, 1 = Infiltrative, 2 = Infiltrative-hyperplastic, 3a = Flat destructive with mild villous atrophy, 3b = Flat destructive with moderate villous atrophy, 3c = Flat destructive with total villous atrophy and 4 = Atrophic-hypoplastic.

FITC–dextran assay

For evaluation of gut permeability, mice were orally gavaged with 4 kDa FITC–dextran (Sigma-Aldrich) after fasting for 4 h. FITC–dextran (100 mg/mL) was dissolved in PBS and gavaged at 44mg/100 g body weight. Four h post gavage, mice were euthanized and blood was collected immediately via cardiac puncture. Serum was isolated and was diluted with an equal volume of PBS, of which 100 μL which was added to a 96-well microplate in duplicate. FITC in blood sera was quantified using florescence spectrometer. The plate was read at an excitation of 485 nm (20 nm band width) and an emission wavelength of 528 nm, and serially diluted FITC-dextran was used to generate a standard curve to calculate serum concentrations. A naive mouse gavaged with PBS for the same duration was used to determine background fluorescence.

LT-specific tetramer production

MHC class II (I-Ab) LTA166-176 tetramers (RYYRNLNIAPA) were produced in our laboratory as previously described (Moon et al., 2007). Peptide:I-Ab molecules were expressed in *Drosophila* S2 cells using the *Drosophila* Expression System kit (Invitrogen). Cells were co-transfected via calcium phosphate with plasmids encoding the I-Ab alpha chain, the I-Ab beta chain, a birA gene, and a blasticidin resistance gene at a molar ratio of 9:9:9:1. Transfected cells were selected in blasticidin-containing media for two weeks at 28°C, passaged into serum-free media, and scaled up to one liter cultures in three liter spinner flasks. When cell densities exceeded 10^7 /mL, expression was induced by the addition of 0.8 mM copper sulfate. Peptide:I-Ab heterodimers were purified from supernatants 8 days later using'' a His-Bind Purification Kit (Millipore Sigma) followed by a Monomeric Avidin Column (Thermo Scientific). The peptide:I-Ab 'monomer' was then separated from the free biotin used to elute from the latter column by multiple washes with 1X PBS over a 30 kDa molecular weight cut-off centrifugal filter unit (Millipore Sigma). Monomer concentration was determined by absorbance at 280nm via a Nanodrop 2000 (Thermo Scientific, extinction coefficient = 0.066 cm-1 uM-1). Monomers created this way contain an 11 amino acid sequence encoding the antigenic peptides LTA166-176 (including the immunogenic nonamer LTA168-176 plus two N-terminal amino acids) was fused to the N terminus of the beta chain via a flexible polyglycine linker (Kozono et al., 1994).

The streptavidin binding efficacy of each monomer is determined by comparing monomer alone and monomer and streptavidin mixed in a molar ratio of 4 monomer: 1 PE-conjugated streptavidin run on a native polyacrylamide gel (Bio-Rad) stained with Coomassie Blue R-250. Tetramers were made by mixing a molar ratio of 4.5 monomer: 1 APC-conjugated streptavidin (Prozyme).

Oral vaccination and isolation of vaccine specific cells

Double mutant *E. coli* heat labile toxin (R192G/L211A) (dmLT), was produced from *E. coli* clones expressing recombinant protein as previously described (Norton et al., 2011). Mice were immunized twice, seven days apart by oral gavage with 20 μg of dmLT on completion of the EED protocol and vaccine responses were assayed two weeks after primary gavage as described before (Hall et al., 2011a). In some experiments mice were treated with antibiotics for three weeks prior to vaccination. Staining of tetramer positive T cells was carried out after magnetic isolation of the cells as described (Moon et al., 2009). Briefly, at the completion of the vaccination protocol, the small intestines of differently treated mice were harvested, cleaned, flayed open and digested to a single cell suspension. Cells were then incubated with the APC-LT166 tetramer at room temperature for an hour to allow binding of dmLT-specific cells, and then subjected to MACS enrichment using the EasySep APC Positive Selection Kit II. Cells were stained as fixed as described in the flow cytometry section.

In vivo ETEC challenge

Mice were challenged with ETEC H10407 Kan^{Res} (ETEC jf876) as shown previously (Roy et al., 2011), with a few modifications. All mice were given streptomycin (5g/liter) in their drinking water 48 h prior to ETEC challenge to eradicate normal resident bacterial flora in the intestinal tract (Wadolkowski et al., 1988). 12 h prior to inoculation, food was withdrawn and antibiotic-treated water was replaced with regular water. 20 min prior to ETEC challenge, mice were gavaged with bicarbonate solution to reduce the effect of stomach acidity on the bacteria. Each mouse was orally inoculated with a suspension of $1x10^4$ ETEC in a final volume of 200 μL via a gavage needle. For isolating mucosa-associated ETEC, a 3cm segment of the terminal ileum, beginning from the ileocecal junction and extending proximally, was removed, opened longitudinally and placed in 2mL of sterile PBS with 0.05% Tween 20. The sample was vortexed for 5 s, incubated for 10 min at room temperature, and vortexed again for 5 s. 100 μL of the resulting suspension was

then plated in duplicate onto Kanamycin/LB agar plates and incubated at 37°C overnight prior to counting of colonies. CUMT8 *E. coli* (gavaged for EED induction prior to ETEC challenge) was susceptible to Kanamycin and did not confound the analysis of the ETEC colonization/protection assay.

In some experiments mice were depleted of CD4 T cells after immunization via IP injection of 200 μg an anti-CD4 antibody (GK1.5 clone) at day 8 and day 11 of the prime/boost oral vaccination protocol.

Antibiotic treatment

The antibiotic cocktail used comprised of Metronidazole (1mg/mL), Ampicillin (1mg/mL), Neomycin (1mg/mL) and Vancomycin (0.5mg/mL) (MANV). Antibiotics were provided in the drinking water and were given to mice for 3 weeks after EED establishment (days 28 to 49 on diets). To reduce the bitter taste of metronidazole and prevent dehydration, antibiotic water was supplemented with 0.5 g/L of saccharin.

qRT-PCR analysis

Real-time RT-PCR (qPCR) was performed using SYBR Green supermix (Bio-RAD) on a CFX Connect Real-time PCR Detection Machine (Bio-RAD). Please see the Key resources table for primer sequences. For evaluation of bacterial abundance, DNA from stool and ileal contents were isolated using QIAamp Fast DNA Stool Mini Kit (QIAGEN). CUMT8 *E. coli* was measured using primers that amplify the FliC gene and number of bacteria calculated against a standard curve prepared from known quantities of CUMT8 *E. coli*. ECMB *E. coli* was identified by PCR identification of a distinct sequence in the OmpL gene. For LCN2 expression, terminal ileums (3cm from ileocecal junction) from ISO and EED mice were homogenized in Trizol buffer (Life Technologies). RNA was transcribed into cDNA using iScript reagent (Bio-RAD) according to manufacturer's instructions. LCN2 expression was normalized to Gapdh and expression level determined by the delta-delta Ct method. Reaction: 95°C for 3 min, 49 cycles at 95°C for 10 s (s) and 60°C for 30 s.

16S rRNA amplicon analysis of relative bacterial abundance

DNA was isolated using the QIAamp Fast DNA Stool Mini Kit (QIAGEN) and the extracted DNA was stored at −20°C prior to 16S amplicon PCR and sequencing. Analysis of small subunit ribosomal RNA gene (16S rRNA) expression was done using following primers;16S primer Fwd: 5′-ACTCCTACGGGAGGCAGCAGT-3′, Rev: 5′-ATTACCGCGGCTGCTGGC-3′. Sequencing was carried out by BGI Genomics. The dataset analyzed is available through NCBI under the accession number PRJNA736663. Microbiome informatics were performed using QIIME2 2020.2 (Bolyen et al., 2019). Raw sequences were quality-filtered and denoised with DADA2 (Callahan et al., 2016). Amplicon variant sequences (ASVs) were aligned with MAFFT (Katoh et al., 2002) and used to construct a phylogeny with FastTree2(Price et al., 2010). Alpha diversity metrics (observed OTUs), beta diversity metrics (Bray Curtis dissimilarity) and Principle Coordinate Analysis (PCoA) were estimated after samples were rarefied to 63,000 (subsampled without replacement) sequences per samples. Clustering of fecal and ileal microbiota samples was performed by PCoA based on bacterial community similarity (using the Bray Curtis/Jaccard algorithm). Taxonomy was assigned to ASVs using naive Bayes taxonomy classifier against the Greengenes 18_8 99% OTUs reference sequences (McDonald et al., 2012). All plots were made with publicly available R packages. The linear discriminant analysis (LDA) effect size (LEfSe) method was use to analyze the intergroup differences at phylum, class, order, family and genus level in each group were analyzed using the default settings on the website (https://huttenhower.sph.harvard.edu/galaxy/root). 2-tailed nonparametric Kruskal-Wallis test (determine significance of differences in OTUs between EED v ALL) and unpaired Wilcoxon test (pairwise test among the two groups) are employed by LEfSe followed by LDA to determine effect size of each differentially abundant OTU (Segata et al., 2011). Results are expressed at mean+/−SEM, where significant differences had a p value < 0.05 and LDA score (log10)>2.4

Flow cytometry

All antibodies used for flow cytometry were purchased from either ThermoFisher, BD Biosciences, or BioLegend and are listed in the key resources table. Dead cells were discriminated in all experiments using LIVE/DEAD fixable dead stain (ThermoFisher). All stains were carried out in media containing anti-CD16/32 blocking antibody (clone 93, ThermoFisher). For intracellular staining, cells were fixed and permeabilized using the FoxP3/Transcription factor staining buffer set according to the manufacturer's directions (ThermoFisher). Intracellular staining for IL-10 production from Treg cells was carried out on siLP cell suspensions treated with PMA/ionomycin/brefeldin A for four h and fixed using Fix/Perm (BD Biosciences). All flow cytometry was acquired on an LSRFortessa FACS analyzer (BD Biosciences) and cell sorting was carried out on a FACS Aria (BD Biosciences). Cells were isolated from the small intestine, Peyer's Patches, spleen and lymph nodes for flow cytometry as described previously (Hand et al., 2012)

Suppression assay

Small intestinal Treg cells (CD45+CD90+CD4+GFP+ T cells) from ISO and EED *Foxp3*$^{DTR\text{-}GFP}$ mice were sorted using the BD FACSAria sorter for comparing suppressive efficacy along with splenic non-Treg cells(CD45+CD90+CD4+GFP− T cells) cells and splenic antigen presenting cells (APCs) (CD45+CD90-) from a naive mouse. Splenic Treg cells (CD45+CD90+CD4+GFP+ T cells) were also sorted as a positive control for suppression. The responder cells (splenic non-Treg cells) from naive *Foxp3*$^{DTR\text{-}GFP}$ mice were labeled with 5 μM CellTrace Violet (Life Technology). Responder cells (4×10^3), APCs (8×10^3), and different concentrations of Treg cells (1:2-1:64 T_{reg}: T_{eff} ratio, 500-2000 Treg cells) were activated with 2 μg/mL anti-CD3 (Biolegend) in a 96-well round bottom

plate with 100 μL RPMI for 72 h (Turnis et al., 2016). Suppression was calculated as previously described (McMurchy and Levings, 2012). Briefly, cells were acquired by the BD LSR Fortessa, and the division index of responder cells was analyzed on the division of CellTrace Violet. Suppression was then calculated with the formula % Suppression = $(1\text{-}DI_{Treg}/DI_{Ctrl}) \times 100\%$ (DI_{Treg} stands for the division index of responder cells with Treg cells, and DI_{Ctrl} stands for the division index of responder cells activated without Treg cells).

Anti-dmLT ELISA

For detection of dmLT-specific IgA antibody from intestinal lavage, 96-well-plates were coated with 1 μg/mL of dmLT protein overnight at 4°C, blocked with 1% BSA for 1 h followed by incubation with intestinal lavage (cleared of solid particles/bacteria by centrifugation) overnight at 4°C. Next day, after washing, IgA antibody bound to dmLT was detected by HRP-labeled anti-IgA antibody and developed using standard ELISA substrate. A naive mouse was used as a negative control.

Luminex assays

Cytokines from ileal homogenates were measured by Luminex according to the manufacturer's instructions using the MILLIPLEX Mouse Th17 Magnetic Bead Panel (Millipore Sigma),

ALDH activity assay

ALDH activity was analyzed using the Aldefluor kit (STEMCELL Technologies) according to the manufacturer's protocol. Briefly, 1×10^6 cells/mL cells were incubated in 15 mL tubes with 5 μL /mL Aldefluor reagent for 30 min in a 37°C water bath with or without the DEAB inhibitor (as a control to determine background). All subsequent washes and staining was done in the assay buffer provided in the kit to prevent Aldefluor loss. Flow cytometric analysis was performed to determine the percent of DCs (Live CD45+ CD11c+ MHCII+) that were Aldefluor+.

Diphtheria toxin (DT) and tamoxifen (TX) administration

Mice were intraperitoneally (I.P.) injected with 25 μg/kg diphtheria toxin (DT, Sigma) twice, with three days between injections (PBS used as vehicle). Tamoxifen (TX, Sigma-Aldrich), was orally gavaged at 5mg/mouse/day, first for five consecutive days to activate the promoter and then once every three days for the duration of the deletion. Since TX is poorly soluble in water, the amount needed for a single day was dissolved in EtOH with heating to 37°C and then diluted in corn oil (Sigma) such that 100ul had 5mg of TX. Corn oil was used for vehicle controls.

QUANTIFICATION AND STATISTICAL ANALYSIS

Due to the necessities of diets and microbiota modification, mouse studies were performed in a non-blinded manner. Data are presented as mean ± SEM. Statistical significance was determined using unpaired Student's t test when comparing two groups, and one-way ANOVA with multiple comparisons, when comparing multiple groups. The Treg suppression assay was analyzed with a 2-way ANOVA. Significance was defined as $p > 0.05$; $^*p \leq 0.05$; $^{**}p \leq 0.01$; $^{***}p \leq 0.001$. All statistical analysis was calculated using Prism software (GraphPad). For details on significance, please see figure legends.